EUROPEAN LABORATORY FOR PARTICLE PHYSICS

CERN-EP/99-043
March 16th, 1999

Search for R-Parity Violating Decays of Scalar Fermions at LEP

The OPAL Collaboration

Abstract

A search for pair produced scalar fermions with couplings that violate R-parity has been performed using a data sample corresponding to an integrated luminosity of 56 pb^{-1} at a centre-of-mass energy of $\sqrt{s}$ = 183 GeV collected with the OPAL detector at LEP. An important consequence of R-parity breaking interactions is that the lightest supersymmetric particle is expected to be unstable. Searches for R-parity violating decays of charged sleptons, sneutrinos and stop quarks have been performed under the assumptions that the lightest supersymmetric particle decays promptly and that only one of the R-parity violating couplings is dominant for each of the decay modes considered. Such processes would yield multi-leptons, jets plus leptons or multi-jets, with or without missing energy, in the final state. No significant excess of such events has been observed. Limits on the production cross-sections of scalar fermions in R-parity violating scenarios are obtained. Mass exclusion regions are also presented in the framework of the Constrained Minimal Supersymmetric Standard Model.

(Submitted to E. Phys. C.)

The OPAL Collaboration

G. Abbiendi[2], K. Ackerstaff[8], G. Alexander[23], J. Allison[16], N. Altekamp[5], K.J. Anderson[9], S. Anderson[12], S. Arcelli[17], S. Asai[24], S.F. Ashby[1], D. Axen[29], G. Azuelos[18,a], A.H. Ball[17], E. Barberio[8], R.J. Barlow[16], J.R. Batley[5], S. Baumann[3], J. Bechtluft[14], T. Behnke[27], K.W. Bell[20], G. Bella[23], A. Bellerive[9], S. Bentvelsen[8], S. Bethke[14], S. Betts[15], O. Biebel[14], A. Biguzzi[5], I.J. Bloodworth[1], P. Bock[11], J. Bohme[14], D. Bonacorsi[2], M. Boutemeur[33], S. Braibant[8], P. Bright-Thomas[1], L. Brigliadori[2], R.M. Brown[20], H.J. Burckhart[8], P. Capiluppi[2], R.K. Carnegie[6], A.A. Carter[13], J.R. Carter[5], C.Y. Chang[17], D.G. Charlton[1,b], D. Chrisman[4], C. Ciocca[2], P.E.L. Clarke[15], E. Clay[15], I. Cohen[23], J.E. Conboy[15], O.C. Cooke[8], J. Couchman[15], C. Couyoumtzelis[13], R.L. Coxe[9], M. Cuffiani[2], S. Dado[22], G.M. Dallavalle[2], R. Davis[30], S. De Jong[12], A. de Roeck[8], P. Dervan[15], K. Desch[8], B. Dienes[32,h], M.S. Dixit[7], J. Dubbert[33], E. Duchovni[26], G. Duckeck[33], I.P. Duerdoth[16], P.G. Estabrooks[6], E. Etzion[23], F. Fabbri[2], A. Fanfani[2], M. Fanti[2], A.A. Faust[30], F. Fiedler[27], M. Fierro[2], I. Fleck[10], A. Frey[8], A. Furtjes[8], D.I. Futyan[16], P. Gagnon[7], J.W. Gary[4], S.M. Gascon-Shotkin[17], G. Gaycken[27], C. Geich-Gimbel[3], G. Giacomelli[2], P. Giacomelli[2], V. Gibson[5], W.R. Gibson[13], D.M. Gingrich[30,a], D. Glenzinski[9], J. Goldberg[22], W. Gorn[4], C. Grandi[2], K. Graham[28], E. Gross[26], J. Grunhaus[23], M. Gruwe[27], C. Hajdu[31], G.G. Hanson[12], M. Hansroul[8], M. Hapke[13], K. Harder[27], A. Harel[22], C.K. Hargrove[7], M. Harin-Dirac[4], M. Hauschild[8], C.M. Hawkes[1], R. Hawkings[27], R.J. Hemingway[6], M. Herndon[17], G. Herten[10], R.D. Heuer[27], M.D. Hildreth[8], J.C. Hill[5], P.R. Hobson[25], A. Hocker[9], K. Hoffman[8], R.J. Homer[1], A.K. Honma[28,a], D. Horvath[31,c], K.R. Hossain[30], R. Howard[29], P. Huntemeyer[27], P. Igo-Kemenes[11], D.C. Imrie[25], K. Ishii[24], F.R. Jacob[20], A. Jawahery[17], H. Jeremie[18], M. Jimack[1], C.R. Jones[5], P. Jovanovic[1], T.R. Junk[6], N. Kanaya[24], J. Kanzaki[24], D. Karlen[6], V. Kartvelishvili[16], K. Kawagoe[24], T. Kawamoto[24], P.I. Kayal[30], R.K. Keeler[28], R.G. Kellogg[17], B.W. Kennedy[20], D.H. Kim[19], A. Klier[26], T. Kobayashi[24], M. Kobel[3,d], T.P. Kokott[3], M. Kolrep[10], S. Komamiya[24], R.V. Kowalewski[28], T. Kress[4], P. Krieger[6], J. von Krogh[11], T. Kuhl[3], P. Kyberd[13], G.D. Lafferty[16], H. Landsman[22], D. Lanske[14], J. Lauber[15], I. Lawson[28], J.G. Layter[4], D. Lellouch[26], J. Letts[12], L. Levinson[26], R. Liebisch[11], B. List[8], C. Littlewood[5], A.W. Lloyd[1], S.L. Lloyd[13], F.K. Loebinger[16], G.D. Long[28], M.J. Losty[7], J. Lu[29], J. Ludwig[10], D. Liu[12], A. Macchiolo[18], A. Macpherson[30], W. Mader[3], M. Mannelli[8], S. Marcellini[2], A.J. Martin[13], J.P. Martin[18], G. Martinez[17], T. Mashimo[24], P. Mattig[26], W.J. McDonald[30], J. McKenna[29], E.A. Mckigney[15], T.J. McMahon[1], R.A. McPherson[28], F. Meijers[8], P. Mendez-Lorenzo[33], F.S. Merritt[9], H. Mes[7], A. Michelini[2], S. Mihara[24], G. Mikenberg[26], D.J. Miller[15], W. Mohr[10], A. Montanari[2], T. Mori[24], K. Nagai[8], I. Nakamura[24], H.A. Neal[12,g], R. Nisius[8], S.W. O'Neale[1], F.G. Oakham[7], F. Odorici[2], H.O. Ogren[12], A. Okpara[11], M.J. Oreglia[9], S. Orito[24], G. Pasztor[31], J.R. Pater[16], G.N. Patrick[20], J. Patt[10], R. Perez-Ochoa[8], S. Petzold[27], P. Pfeifenschneider[14], J.E. Pilcher[9], J. Pinfold[30], D.E. Plane[8], P. Poffenberger[28], B. Poli[2], J. Polok[8], M. Przybycien[8,e], A. Quadt[8], C. Rembser[8], H. Rick[8], S. Robertson[28], S.A. Robins[22], N. Rodning[30], J.M. Roney[28], S. Rosati[3], K. Roscoe[16], A.M. Rossi[2], Y. Rozen[22], K. Runge[10], O. Runolfsson[8], D.R. Rust[12], K. Sachs[10], T. Saeki[24], O. Sahr[33], W.M. Sang[25], E.K.G. Sarkisyan[23], C. Sbarra[29], A.D. Schaile[33], O. Schaile[33], P. Scharff-Hansen[8], J. Schieck[11], S. Schmitt[11], A. Schoning[8], M. Schroder[8], M. Schumacher[3], C. Schwick[8], W.G. Scott[20], R. Seuster[14], T.G. Shears[8], B.C. Shen[4], C.H. Shepherd-Themistocleous[8], P. Sherwood[15], G.P. Siroli[2], A. Sittler[27], A. Skuja[17], A.M. Smith[8], G.A. Snow[17], R. Sobie[28], S. Soldner-Rembold[10,f], S. Spagnolo[20], M. Sproston[20], A. Stahl[3], K. Stephens[16], J. Steuerer[27], K. Stoll[10], D. Strom[19], R. Strohmer[33], B. Surrow[8],

S.D. Talbot[1], P. Taras[18], S. Tarem[22], R. Teuscher[9], M. Thiergen[10], J. Thomas[15], M.A. Thomson[8], E. Torrence[8], S. Towers[6], I. Trigger[18], Z. Trocsanyi[32], E. Tsur[23], M.F. Turner-Watson[1], I. Ueda[24], R. Van Kooten[12], P. Vannerem[10], M. Verzocchi[8], H. Voss[3], F. Wackerle[10], A. Wagner[27], C.P. Ward[5], D.R. Ward[5], P.M. Watkins[1], A.T. Watson[1], N.K. Watson[1], P.S. Wells[8], N. Wermes[3], D. Wetterling[11] J.S. White[6], G.W. Wilson[16], J.A. Wilson[1], T.R. Wyatt[16], S. Yamashita[24], V. Zacek[18], D. Zer-Zion[8]

[1]School of Physics and Astronomy, University of Birmingham, Birmingham B15 2TT, UK
[2]Dipartimento di Fisica dell' Universita di Bologna and INFN, I-40126 Bologna, Italy
[3]Physikalisches Institut, Universitat Bonn, D-53115 Bonn, Germany
[4]Department of Physics, University of California, Riverside CA 92521, USA
[5]Cavendish Laboratory, Cambridge CB3 0HE, UK
[6]Ottawa-Carleton Institute for Physics, Department of Physics, Carleton University, Ottawa, Ontario K1S 5B6, Canada
[7]Centre for Research in Particle Physics, Carleton University, Ottawa, Ontario K1S 5B6, Canada
[8]CERN, European Organisation for Particle Physics, CH-1211 Geneva 23, Switzerland
[9]Enrico Fermi Institute and Department of Physics, University of Chicago, Chicago IL 60637, USA
[10]Fakultat fur Physik, Albert Ludwigs Universitat, D-79104 Freiburg, Germany
[11]Physikalisches Institut, Universitat Heidelberg, D-69120 Heidelberg, Germany
[12]Indiana University, Department of Physics, Swain Hall West 117, Bloomington IN 47405, USA
[13]Queen Mary and Westfield College, University of London, London E1 4NS, UK
[14]Technische Hochschule Aachen, III Physikalisches Institut, Sommerfeldstrasse 26-28, D-52056 Aachen, Germany
[15]University College London, London WC1E 6BT, UK
[16]Department of Physics, Schuster Laboratory, The University, Manchester M13 9PL, UK
[17]Department of Physics, University of Maryland, College Park, MD 20742, USA
[18]Laboratoire de Physique Nucleaire, Universite de Montreal, Montreal, Quebec H3C 3J7, Canada
[19]University of Oregon, Department of Physics, Eugene OR 97403, USA
[20]CLRC Rutherford Appleton Laboratory, Chilton, Didcot, Oxfordshire OX11 0QX, UK
[22]Department of Physics, Technion-Israel Institute of Technology, Haifa 32000, Israel
[23]Department of Physics and Astronomy, Tel Aviv University, Tel Aviv 69978, Israel
[24]International Centre for Elementary Particle Physics and Department of Physics, University of Tokyo, Tokyo 113-0033, and Kobe University, Kobe 657-8501, Japan
[25]Institute of Physical and Environmental Sciences, Brunel University, Uxbridge, Middlesex UB8 3PH, UK
[26]Particle Physics Department, Weizmann Institute of Science, Rehovot 76100, Israel
[27]Universitat Hamburg/DESY, II Institut fur Experimental Physik, Notkestrasse 85, D-22607 Hamburg, Germany
[28]University of Victoria, Department of Physics, P O Box 3055, Victoria BC V8W 3P6, Canada
[29]University of British Columbia, Department of Physics, Vancouver BC V6T 1Z1, Canada
[30]University of Alberta, Department of Physics, Edmonton AB T6G 2J1, Canada
[31]Research Institute for Particle and Nuclear Physics, H-1525 Budapest, P O Box 49, Hungary

[32] Institute of Nuclear Research, H-4001 Debrecen, P O Box 51, Hungary
[33] Ludwigs-Maximilians-Universitat Munchen, Sektion Physik, Am Coulombwall 1, D-85748 Garching, Germany

[a] and at TRIUMF, Vancouver, Canada V6T 2A3
[b] and Royal Society University Research Fellow
[c] and Institute of Nuclear Research, Debrecen, Hungary
[d] on leave of absence from the University of Freiburg
[e] and University of Mining and Metallurgy, Cracow
[f] and Heisenberg Fellow
[g] now at Yale University, Dept of Physics, New Haven, USA
[h] and Depart of Experimental Physics, Lajos Kossuth University, Debrecen, Hungary.

1 Introduction

In Supersymmetric (SUSY) [1] models each elementary particle is accompanied by a supersymmetric partner whose spin differs by half a unit. Most of the searches for these supersymmetric particles ("sparticles") are performed within the Minimal Supersymmetric extension of the Standard Model (MSSM) [2], assuming R-parity conservation. R-parity [3] is a new multiplicative quantum number defined as $R_p = (-1)^{2S+3B+L}$ where S, B and L are the spin, baryon and lepton number of the particle, respectively. R-parity discriminates between ordinary and supersymmetric particles: $R_p = +1$ for the Standard Model particles and $R_p = -1$ for their supersymmetric partners. R-parity conservation implies that supersymmetric particles are always pair produced and always decay through cascade decays to ordinary particles and the lightest supersymmetric particle (LSP). In this context, the LSP is often assumed to be the lightest neutralino, $\tilde{\chi}_1^0$, which is then expected to be stable and to escape detection due to its weakly interacting nature. The characteristic signature of the supersymmetric R-parity conserving decays is therefore missing energy.

In this paper, the possible direct manifestations of R-parity breaking couplings via processes with distinct signatures are studied. If R-parity is violated, sparticles can decay directly to Standard Model particles. Therefore, the signatures sought in the analyses of this paper differ from the missing energy signatures of R-parity conserving processes.

With the MSSM particle content, R-parity violating interactions are parametrised with a gauge-invariant superpotential that includes the following Yukawa coupling terms [4]:

$$W_{RPV} = \lambda_{ijk} L_i L_j \overline{E}_k + \lambda'_{ijk} L_i Q_j \overline{D}_k + \lambda''_{ijk} \overline{U}_i \overline{D}_j \overline{D}_k ; \qquad (1)$$

where i,j,k are the generation indices of the superfields L, Q, E, D and U. L and Q are lepton and quark left-handed doublets, respectively. $\overline{E}$, $\overline{D}$ and $\overline{U}$ are right-handed singlet charge-conjugate superfields for the charged leptons and down- and up-type quarks, respectively. The interactions corresponding to these superpotential terms are assumed to respect the gauge symmetry $SU(3)_C \otimes SU(2)_L \otimes U(1)_Y$ of the Standard Model. The λ_{ijk} are non-vanishing only if $i < j$, so that at least two different generations are coupled in the purely leptonic vertices. The λ''_{ijk} are are non-vanishing only for for $j < k$. The λ and λ' couplings both violate lepton number (L) conservation and the λ'' couplings violate baryon number (B) conservation. There are nine λ couplings for the triple lepton vertices, 27 λ' couplings for the lepton-quark-quark vertices and nine λ'' couplings for the triple quark vertices. There are therefore a total of 45 new R-parity violating couplings. In the constrained MSSM framework [1], there are five initial parameters completely determining all sparticle masses and couplings.

Recently, supersymmetric models with R-parity violation (RPV) have attracted considerable theoretical and phenomenological interest (see for instance [4]). Indeed, there exist no theoretical or experimental arguments excluding R-parity violation [5, 6, 7]. Therefore, it is important to consider the phenomenology of possible R-parity violating scenarios. The branching ratios of some of the R-parity violating decay modes can be comparable or even larger than R-parity conserving modes. For example, this could be the case for the scalar top quark ("stop") decay modes to third-generation fermions.

[1] The constrained MSSM implies a common gaugino mass and a common sfermion mass at the GUT scale.

From the experimental point of view, there are several upper bounds[2] on the R-parity violating Yukawa couplings, λ, λ' and λ''. A list of upper limits on individual couplings can be found in [8, 9, 10, 11, 12]. Most of the upper limits on the couplings are of $O(10^{-2})$, but there also exist some more stringent limits. For instance, $\lambda'_{111} < 10^{-4}$ from neutrinoless double beta decay [13], $\lambda''_{112} < 10^{-6}$ [14] from double nucleon decay and $\lambda''_{113} < 10^{-4}$ [14] from limits on $n - \bar{n}$ oscillation. Most of the couplings are constrained by experimental results but most of these upper bounds are still high compared to the sensitivity attainable with direct searches at LEP (of $O(10^{-5})$). Furthermore the simultaneous presence of the couplings λ'' (B-violating) and λ' (L-violating) is forbidden since it would allow fast squark-mediated proton decay at tree level. The experimental non-observation of proton decay places strong bounds on the product of these two couplings, i.e., $\lambda'\lambda'' < 10^{-10}$ [15].

Although pair production is not required with R-parity violation, only searches for R-parity violating decays of pair-produced scalar fermions ("sfermions"), such as the charged and neutral scalar leptons and scalar top quark, are presented in this paper. Their production is fully determined by gauge couplings and their masses. Supersymmetric particles can also be singly produced and, for example, indirect limits from the OPAL two-fermion pair-production cross-section measurements are given in [16].

Two different scenarios are probed. In the first scenario, the decays of sfermions via the lightest neutralino, $\tilde{\chi}^0_1$, are considered, where $\tilde{\chi}^0_1$ is treated as the LSP and assumed to decay via an R-parity violating interaction. These are denoted "indirect decays". SUSY cascade decays via particles other than the LSP are not considered. In the second scenario, "direct" decays of sparticles to Standard Model particles are investigated. In this case, the sparticle considered is assumed to be the LSP, such that R-parity conserving decay modes do not contribute. In both scenarios, it is assumed that only one of the 45 Yukawa-like couplings is non zero at a time.

Only values of the Yukawa-like λ-couplings larger than $O(10^{-5})$ are relevant to this analysis. For smaller couplings, the lifetime of sparticles would be sufficiently long to produce a secondary decay vertex, clearly detached from the primary vertex, or even outside the detector. These topologies have not been considered in this paper, but decays outside the detector have been treated elsewhere [17].

In this paper, the data produced in e^+e^- collisions at LEP and collected with the OPAL detector during 1997 at a centre-of-mass energy of $\sqrt{s} \simeq 183$ GeV are analysed. These data correspond to an integrated luminosity of about 56 pb^{-1}. The production and R-parity violating decays of $\tilde{\nu}$, $\tilde{\chi}^0_1$ via λ and λ' and $\tilde{t}$ via λ' and λ'' are described in Section 2, together with the possible signal topologies resulting from these processes. The signal and background Monte Carlo simulations used in the different analyses are described in Section 3, and a short description of the OPAL detector follows in Section 4. Sections 5, 6, 7, 8 and 9 describe the specific analyses optimised to search for R-parity violating processes. The physics interpretation is given in Section 10 which presents cross-section limits and interpretations in the MSSM.

2 Sparticle Production and Decays

In this section, the production and decay modes of different sfermion species are discussed. The decay modes that result from λ, λ' and λ'' couplings are presented. Table 1 summarises

[2] All quoted limits are given for a sparticle mass of 100 GeV.

the production and decay mechanisms as well as the coupling involved in the decay, the final state topologies searched for, and the analysis names as used in Sections 5, 6, 7, 8 and 9. In the indirect decays, the particles resulting from the $\tilde{\chi}_1^0$ decay are put in parentheses.

Production and Decay		Coupling	Topology	Analysis
$\tilde{\nu}\bar{\tilde{\nu}}$!	$\nu\bar{\nu}$	direct	2 ℓ + E_{miss}	(A) 5.2
$\tilde{\ell}\tilde{\ell}$! $\tilde{\chi}_1^0\tilde{\chi}_1^0$!	($\ell\nu\nu$) ($\ell\nu\nu$)	indirect	4 ℓ + E_{miss}	(B) 5.3
$\tilde{\ell}\tilde{\ell}$!	$\ell\nu\ell^+\nu$	direct	4 ℓ	(C) 5.3
$\tilde{\nu}\bar{\tilde{\nu}}$! $\nu\tilde{\chi}_1^0\bar{\nu}\tilde{\chi}_1^0$!	ν($\ell\nu\nu$) $\bar{\nu}$($\ell\nu\nu$)	indirect	6 ℓ + E_{miss}	(D) 5.4
$\tilde{t}_1\bar{\tilde{t}}_1$!	$e^+qe\bar{q}$	^{0} direct	2 e + 2 jets	(E) 6.1
$\tilde{t}_1\bar{\tilde{t}}_1$!	$^+q\bar{q}$	^{0} direct	2 + 2 jets	(E) 6.1
$\tilde{t}_1\bar{\tilde{t}}_1$!	$^+q\bar{q}$	^{0} direct	2 + 2 jets	(F) 6.2
$\tilde{}^+\tilde{}$! $^+\tilde{\chi}_1^0\bar{}\tilde{\chi}_1^0$!	$^+$('qq) ('qq)	^{0} indirect	+ jets	(F) 7.2
	$^+$(qq) ('qq)	^{0} indirect	+ jets	(F) 7.2
	$^+$(qq) (qq)	^{0} indirect	+ jets	(F) 7.2
$\tilde{\nu}\bar{\tilde{\nu}}$! $\nu\tilde{\chi}_1^0\bar{\nu}\tilde{\chi}_1^0$!	ν('qq) $\bar{\nu}$('qq)	^{0} indirect	ℓ + jets	(G) 7.1
	ν(qq) $\bar{\nu}$('qq)	^{0} indirect	ℓ + jets	(G) 7.1
	ν(qq) $\bar{\nu}$(qq)	^{0} indirect	ℓ + jets	(G) 7.1
$\tilde{\ell}\bar{\tilde{\ell}}$! $\tilde{\chi}_1^0\tilde{\chi}_1^0$!	(qq) (qq)	^{0} indirect	4 jets + E_{miss}	(H) 8
$\tilde{\ell}\bar{\tilde{\ell}}$!	$qq\bar{q}\bar{q}$	^{0} direct	4 jets	(I) 9.1
$\tilde{\nu}\bar{\tilde{\nu}}$!	$qq\bar{q}\bar{q}$	^{0} direct	4 jets	(I) 9.1
qqq !	$qq\bar{q}\bar{q}$	$^\infty$ direct	4 jets	(I) 9.2

Table 1: List of production and decay mechanisms of the channels that are covered by the various analyses described in this paper. The couplings and decay type searched for in each analysis and the corresponding topologies are described in the second and third columns, respectively. The corresponding section number is indicated in the last column.

The charged lepton, ℓ, is either an electron or a muon. Different analyses are applied when the charged lepton is an electron or a muon (denoted "electron channel" and "muon channel") or when it is a tau (denoted "tau channel"). Each analysis is optimised regarding the number of jets or charged leptons expected in the final states.

If the mass of the scalar charged lepton ("slepton") is less than the beam energy, sleptons may be pair produced in electron-positron collisions through s-channel processes involving a Z^0 or a . Scalar electrons ("selectrons," $\tilde{e}$) may also be produced through t-channel neutralino exchange. This may enhance their production cross-section compared to those for the scalar muons ("smuons," $\tilde{\mu}$) and scalar taus ("staus," $\tilde{\tau}$). Similarly, neutral scalar leptons ("sneutrinos") may be pair-produced via the s-channel or through t-channel chargino exchange.

Sleptons and sneutrinos may decay directly to Standard Model particles through the $_{ijk}L_iL_j\bar{E}_k$ operator. The possible decays are:

$$\tilde{\nu}_{iL} \to \bar{}_j\,\ell_k, \quad \tilde{\nu}_{jL} \to \bar{}_i\,\ell_k, \quad \tilde{\nu}_{kR} \to \ _i\,\ell_j\ ;\ _j\,\ell_i$$

$$\tilde{}_i \to \ ^+_j\,\nu_k, \quad \tilde{}_j \to \ ^+_i\,\bar{\nu}_k$$

where $\tilde{\nu}_{iL}$ denotes a left-handed slepton of the i^{th} generation and $\tilde{\nu}_{kR}$ denotes a right-handed slepton of the k^{th} generation.

If the slepton or sneutrino decays directly via the $\lambda'_{ijk} L_i Q_j \bar{D}_k$ operator[3], the decay modes are:

$$\tilde{\nu}_{iL} \to \bar{u}_j d_k, \quad \tilde{e}_{iL} \to \bar{d}_j d_k$$

where d_k denotes a down-type quark of the k^{th} generation, u_j denotes an up-type quark of the j^{th} generation and d_j denotes a down-type quark of the j^{th} generation.

Sleptons and sneutrinos may also decay indirectly to $\tilde{\chi}_1^0$ plus the corresponding charged or neutral lepton[4]:

$$\tilde{\nu} \to \tilde{\chi}_1^0 \nu, \quad \tilde{e} \to \tilde{\chi}_1^0 e$$

The $\tilde{\chi}_1^0$ may subsequently decay violating R-parity with a λ, λ' or λ'' coupling through an intermediate slepton or sneutrino. In the case of a non-vanishing λ coupling, the $\tilde{\chi}_1^0$ decays proceeding via the $\lambda_{ijk} L_i L_j \bar{E}_k$ operator are:

$$\tilde{\chi}_1^0 \to \nu_i e_j e_k, \quad \tilde{\chi}_1^0 \to \nu_i \bar{e}_j \nu_k, \quad \tilde{\chi}_1^0 \to e_i \nu_j e_k, \quad \tilde{\chi}_1^0 \to \bar{e}_i \nu_j \nu_k$$

In the case of a non-vanishing λ' coupling, the $\tilde{\chi}_1^0$ decays proceeding via the $\lambda'_{ijk} L_i Q_j \bar{D}_k$ operator are:

$$\tilde{\chi}_1^0 \to \nu_i u_j \bar{d}_k, \quad \tilde{\chi}_1^0 \to \nu_i \bar{u}_j d_k, \quad \tilde{\chi}_1^0 \to e_i d_j \bar{d}_k, \quad \tilde{\chi}_1^0 \to \bar{e}_i \bar{d}_j d_k,$$

In the case of a non-vanishing λ'' coupling, the $\tilde{\chi}_1^0$ decays proceeding via the $\lambda''_{ijk} \bar{U}_i \bar{D}_j \bar{D}_k$ operator are:

$$\tilde{\chi}_1^0 \to u_i d_j d_k, \quad \tilde{\chi}_1^0 \to \bar{u}_i \bar{d}_j \bar{d}_k$$

If the mass of the scalar top quark (\stop") is smaller than the beam energy, stop quarks may be produced in pairs in e^+e^- collisions via s-channel Z^0 or γ exchange. Due to the mixing of the left- and right-handed stop, $\tilde{t}_L$ and $\tilde{t}_R$, the observable $\tilde{t}_1 = \tilde{t}_L \cos\theta_t + \tilde{t}_R \sin\theta_t$ could become very light, even the lightest supersymmetric particle. The coupling of the $\tilde{t}_1$ to the Z^0 boson is determined by the mixing angle θ_t, whose value is determined by the top quark mass and the soft SUSY breaking parameters. The $\tilde{t}_1$ decouples from the Z^0 if $\cos^2\theta_t = \frac{4}{3}\sin^2\theta_W$ ($\theta_t \simeq 0.98$ radian), where θ_W is the effective weak mixing angle. For this value of θ_t, $\tilde{t}_1\tilde{t}_1$ may only be produced via a virtual γ and the expected cross-section is therefore reduced.

For the purpose of R-parity violating searches, the stop quark is assumed to be the lightest supersymmetric particle and only direct decays are considered. Only 9 of the 27 λ' parameters are relevant: λ'_{i3k}, $i,k = 1,2,3$, as the stop is contained in the SU(2) doublet field but not in the down type singlet field.

If the stop decays via the $\lambda'_{ijk} L_i Q_j \bar{D}_k$ operator, the decay modes are:

[3] Right-handed sleptons cannot decay via the operator $\lambda'_{ijk} L_i Q_j \bar{D}_k$.

[4] Decays like $\tilde{\nu} \to \tilde{\chi}_2^0 \nu$ or $\tilde{\nu} \to \tilde{\chi}_1^\pm e^\mp$ are not considered here but the appropriate branching ratios are taken into account for interpretation of the results.

$$\tilde{t}_{jL} \;!\; \nu_i^{+} d_k$$

If the stop decays via the $\lambda''\overline{U}_i\overline{D}_j\overline{D}_k$ operator, the decay modes are:

$$\tilde{t}_{iR} \;!\; \overline{d}_j\,\overline{d}_k$$

Under the assumption of R-parity violation, the strength of the coupling and the decay width of a sfermion are determined only by its mass and the λ, λ' and λ'' parameters if the sparticle is the LSP. If the sparticle is not the LSP, both the R-parity conserving and the R-parity violating decay modes are accessible.

In the analyses described in this paper, tracks are required to come from the interaction vertex. Analyses would become inefficient for decay lengths larger than some centimeters. For very long lifetimes, the LSP decays outside the detector, and in the case it is neutral, the event topology would be exactly the same as the R_p conserving case.

For sleptons and sneutrinos, the decay widths are given by [18, 19]:

$$(\tilde{\nu}_i \;!\; \overline{\ell}_j\,\ell_k;\tilde{\nu}_i \;!\; \nu_j^{+}\,\ell_k) = \frac{1}{16}\,\lambda^{2}_{ijk} m_{\tilde{\nu}}\,; \qquad (\tilde{\nu}_i \;!\; \overline{u}_j d_k;\tilde{\nu}_i \;!\; d_j d_k) = \frac{3}{16}\,\lambda'^{2}_{ijk} m_{\tilde{\nu}}\,;$$

neglecting quark and lepton masses.

Similarly, the R-parity violating decay of the stop has a decay width [20] of:

$$(\tilde{t}_L \;!\; \nu_i^{+} d_k) = \frac{1}{16}\,\lambda''^{2}_{i3k} m_t$$

Under the conservative assumptions of a sparticle mass of 45 GeV[5] and a decay length of 0.1 mm the analyses presented in this paper would be sensitive to couplings larger than $O(10^{-5})$.

3 Monte Carlo Simulation

Monte Carlo samples corresponding to the charged slepton, sneutrino and stop pair-production processes as well as Monte Carlo samples used to estimate the background levels due to Standard Model processes were simulated. All generated events were processed through the full simulation of the OPAL detector [21], and the same analysis chain was applied to simulated events as to the data.

The simulation of the signal events has been done at $\sqrt{s} = 183$ GeV with the Monte Carlo program SUSYGEN [22]. Charged and neutral sleptons decaying directly or indirectly via λ or λ' have been produced for the mass values of 45, 70 and 90 GeV. Five masses (45, 60, 75, 80 and 90 GeV) were used for the sneutrino direct decays via λ'. Stop events were simulated at 6 different stop masses (45, 55, 65, 75, 85 and 90 GeV). Samples of 1000 or 2000 events were generated for each relevant coupling.

[5] This number takes into account the indirect limits obtained from the study of the Z^0 width at LEP1.

For the indirect decays, events were produced with $m = m_{\tilde{f}} - m_{\tilde{\chi}^0_1} = m_{\tilde{f}}/2$. Additional samples were simulated for $m_{\tilde{f}} = 90$ GeV and $m = m_{\tilde{f}} - m_{\tilde{\chi}^0_1} = 5$ GeV to account for changes in the event topologies from the model parameters. The values of m were chosen to cover a large range for a limited number of Monte Carlo events. To estimate the systematic errors related to different gaugino mixings, extra samples of pair-produced selectrons and electron-sneutrinos were simulated with five different sets of SUSY parameters.

Events were produced for each of the nine possible couplings. Events were also simulated for each lepton flavour corresponding to the first index of ^{0}. The quark flavour corresponding to the second and third index of ^{0} were fixed to the first and second generation, with a few samples containing bottom qaurks for systematic checks.

For the stop decaying via the ^{0} coupling into a quark and a lepton all nine combinations of quark and lepton flavours in the final state were generated. The production and decay of the stop is simulated as described in [23]. The stops are hadronised to form colourless hadrons and associated fragmentation particles, according to the Lund string fragmentation scheme (JETSET 7.4) [24, 25]. For the decay, a colour string was stretched between the spectator quark and the quark from the stop decay. Further hadronisation was also done using the Lund scheme. The fragmentation function of Peterson [26] has been used. Events were simulated with the mixing angle $_t$ set to zero.

The main sources of background arise from Standard Model four-fermion, two-photon and two-fermion (lepton-pair and multi-hadronic) processes. For two-photon processes, the PHOJET [27] and HERWIG [28] generators have been used to simulate hadronic final states. The Vermaseren [29] generator was used to estimate the background contribution from all two-photon $e^+e^-\nu^+\nu^-$ final states. All other four-fermion final states, other than two-photon $e^+e^-\nu^+\nu^-$, were simulated with grc4f [30], which takes into account all interfering four-fermion diagrams. For the two-fermion final states, BHWIDE [31] was used for the $ee(\ )$ final state and KORALZ [32] for the and the states. The multi-hadronic events, $qq(\ )$, were simulated using PYTHIA [24].

For small contributions to background final states with six or more primary fermions, no Monte Carlo generator exists. These final states are therefore not included in the background Monte Carlo samples. Consequently, the background could be slightly underestimated, which would lead to a conservative approach when calculating upper bounds applying background subtraction.

4 The OPAL Detector

A complete description of the OPAL detector can be found in Ref. [33] and only a brief overview is given here.

The central detector consists of a system of tracking chambers providing charged particle tracking over 96% of the full solid angle[6] inside a 0.435 T uniform magnetic field parallel to the beam axis. It is composed of a two-layer silicon microstrip vertex detector, a high precision drift chamber, a large volume jet chamber and a set of z chambers measuring the track coordinates

[6] The OPAL coordinate system is defined so that the z axis is in the direction of the electron beam, the x axis is horizontal and points towards the centre of the LEP ring, and and are the polar and azimuthal angles, defined relative to the +z- and +x-axes, respectively. The radial coordinate is denoted as r.

along the beam direction. A lead-glass electromagnetic (EM) calorimeter located outside the magnet coil covers the full azimuthal range with excellent hermeticity in the polar angle range of $|\cos\theta| < 0.82$ for the barrel region and $0.81 < |\cos\theta| < 0.984$ for the endcap region. The magnet return yoke is instrumented for hadron calorimetry (HCAL) and consists of barrel and endcap sections along with pole tip detectors that together cover the region $|\cos\theta| < 0.99$. Four layers of muon chambers cover the outside of the hadron calorimeter. Electromagnetic calorimeters close to the beam axis complete the geometrical acceptance down to 24 mrad, except for the regions where a tungsten shield is present to protect the detectors from synchrotron radiation. These include the forward detectors (FD) which are lead-scintillator sandwich calorimeters and, at smaller angles, silicon tungsten calorimeters (SW) [34] located on both sides of the interaction point. The gap between the endcap EM calorimeter and the FD is instrumented with an additional lead-scintillator electromagnetic calorimeter, called the gamma-catcher.

To be considered in the analyses, tracks in the central detector and clusters in the electromagnetic calorimeter were required to satisfy the normal quality criteria employed in OPAL's analysis of Standard Model (SM) lepton pairs [35].

5 Multi-lepton Final States

This section describes the searches for purely leptonic final states that may result from pair production of neutralino or charged sleptons, involving subsequent direct or indirect decays (see Table 1).

5.1 Event and Track Selection

The event preselection and lepton identification are described in [36]. Multi-hadronic, cosmic and Bhabha scattering events were vetoed [36].

At the preselection level, it was also required that the ratio of the number of tracks satisfying the quality criteria described in [35] to the total number of reconstructed tracks be greater than 0.2 to reduce backgrounds from beam-gas and beam-wall events. The visible energy, the visible mass and the total transverse momentum of the event were calculated using the method described in [37]. Finally, the number of good charged tracks was required to be at least two.

Only tracks with $|\cos\theta| < 0.95$ were considered for lepton identification. A track was considered "isolated" if the total energy of other charged tracks within 10° of the lepton candidate was less than 2 GeV. A track was selected as an electron candidate if one of the following three algorithms was satisfied: (i) the output probability of the neural net algorithm described in [38] was larger than 0.8; (ii) the electron selection algorithm as described in [39] for the barrel region or in [40] for the endcap region was satisfied; (iii) $0.5 < E/p < 2.0$, where p is the momentum of the electron candidate and E is the energy of the electromagnetic calorimeter cluster associated with the track. A track was selected as a muon candidate according to the criteria employed in OPAL's analysis of Standard Model muon pairs [35]. That is, the track had associated activity in the muon chambers or hadron calorimeter strips or it had a high momentum but was associated with only a small energy deposit in the electromagnetic calorimeter. Tau candidates were selected by requiring that there were at most three tracks within a 35° cone. The invariant mass computed using all good tracks and EM clusters within

the above cone had to be less than 3 GeV. For muon and electron candidates, the momentum was estimated from the charged track momentum measured in the central detector, while for tau candidates the momentum was estimated from the vector sum of the measured momenta of the charged tracks within the tau cone.

Tracks resulting from photon conversion were rejected using the algorithm described in [41]. For the two- and six-lepton final states, the large background from two-photon processes was reduced by requiring that the total energy deposited in each silicon tungsten calorimeter be less than 5 GeV, be less than 5 GeV in each forward calorimeter, and be less than 5 GeV in each side of the gamma-catcher. In addition to the requirement that there be no unassociated electromagnetic cluster with an energy larger than 25 GeV in the event, it was also required that there be no unassociated hadronic clusters with an energy larger than 10 GeV.

5.2 Final States with Two Leptons plus Missing Energy

Final states with two charged leptons and missing energy may result from direct slepton decays via a coupling. The analysis was optimised to retain good signal efficiency while reducing the background, mainly due to "" final states from W^+W production and to two-photon processes. The following criteria were applied in addition to those described in Section 5.1.

(A 1) Events had to contain exactly two identified and oppositely-charged leptons, each with a transverse momentum with respect to the beam axis greater than 2 GeV.

(A 2) The background from two-photon processes and "radiative return" events ($e^+e \to Z$, where the escapes down the beam pipe) was reduced by requiring that the polar angle of the missing momentum, $_{miss}$, satisfy $|\cos _{miss}| < 0.9$.

(A 3) To reduce further the residual background from Standard Model lepton pair events, it was required that $m_{vis}/\sqrt{s} < 0.80$, where m_{vis} is the event visible mass.

(A 4) The acoplanarity angle[7] ($_{acop}$) between the two leptons was required to be greater than 10 in order to reject Standard Model leptonic events, and smaller than 175 in order to reduce the background due to photon conversions. The acoplanarity angle distribution is shown in Figure 1 (a) after cuts (A 1) to (A 3). The acollinearity angle[8] ($_{acol}$) was also required to be greater than 10 and smaller than 175 .

(A 5) Cuts on a_t^{miss} and p_t^{miss} were applied; a_t^{miss} is the component of the missing momentum vector perpendicular to the event thrust axis in the plane transverse to the beam axis and p_t^{miss} is the missing transverse momentum. The cuts on a_t^{miss} and p_t^{miss} are complementary and reject some two-photon events with high transverse momentum. The full description of these cuts can be found in [36].

In order to maximise the detection efficiencies, events were accepted if they passed the above selection criteria or if they passed the selection of W^+W pair events [42] where both

[7] The acoplanarity angle, $_{acop}$, is defined as 180 minus the angle between the two lepton momentum vectors projected into the x y plane.

[8] The acollinearity angle, $_{acol}$, is defined as 180 minus the space-angle between the two lepton momentum vectors.

W 's decay leptonically. The preselection and detector status criteria described in Section 5.1 were imposed in both cases. There are 75 events selected with 79.7 events expected from all Standard Model processes considered (75.2 from W^+W^- events).

(A 6) At this stage the background from two-photon processes and W^+W^- production was reduced by categorizing the events in different classes according to the flavour of the leptons expected in the final state, as can be seen in Table 2. Events were further selected by applying cuts on the momentum of the two leptons as described in [36] in both the right- and left-handed slepton searches.

Final State			E . (%)	Selected Events	Tot. bkg MC	4-f
		ee + E_{Tmiss}	58{76	11	13.8	13.5
		+ E_{Tmiss}	57{81	10	11.3	11.0
		+ E_{Tmiss}	30{50	10	15.5	12.5
ee or e	or	+ E_{Tmiss}	65{80	39	52.2	51.0
ee or e	or	+ E_{Tmiss}	58{71	39	51.9	48.6
or	or	+ E_{Tmiss}	58{72	40	52.0	48.6

Table 2: Detection efficiencies (in %), events selected and background predicted for the lepton-pair plus missing energy channel and for slepton masses between 45 and 90 GeV. The deficit of events selected in the data compared to the background expectations is interpreted as a downward statistical fluctuation. The number of events in the last three rows are largely correlated, as many final states are shared.

The detection efficiencies are summarised in Table 2. The efficiencies are quoted for slepton masses between 45 and 90 GeV. Detection efficiencies were estimated separately for right- and left-handed e, ~ and ~. The first three lines of Table 2 refer to left-handed sleptons while the other lines refer to right-handed sleptons. Indeed, due to the structure of the corresponding term in the Lagrangian of equation (1), these particles are expected to yield different final states. The expected background from all Standard Model processes considered is normalised to the data luminosity of 56.5 pb^{-1}. As can be seen in Table 2, most of the background remaining comes from 4-fermion processes, expected to be dominated by W^+W^- doubly-leptonic decays.

Due to beam-related backgrounds and to incomplete modelling of two-photon processes, there is poor agreement between the data and Monte Carlo expectation in the early stages of some of the analyses. When the two-photon processes have been effectively reduced after specific cuts (for instance, a cut on the missing transverse momentum), the agreement between data and Monte Carlo is good.

5.3 Final States with Four Leptons with or without Missing Energy

Final states with four charged leptons and no missing energy may result from direct sneutrino decays while the final states with missing energy may result from indirect sneutrino decays via a coupling. Two analyses have been developed and optimised separately for these two

nal states. No specic cut on the lepton avour present in the nal state was applied. To be independent of the type of decay and coupling the two analyses were at the end combined.

The following criteria were applied to select a possible signal in the four leptons plus missing energy topology:

(B 1) Events were required to have at least three charged tracks with a transverse momentum with respect to the beam axis greater than 1.0 GeV.

(B 2) The event transverse momentum calculated without the hadron calorimeter was required to be larger than 0.07 $\sqrt{s}$. This distribution is shown in Figure 1 (b) after cut (B 1) has been applied.

(B 3) Events had to contain at least three identied isolated leptons each with a transverse momentum with respect to the beam axis greater than 1.5 GeV.

(B 4) It was also required that $E_{vis}/\sqrt{s} < 1.1$, where E_{vis} is the event visible energy.

(B 5) The total leptonic energy, dened as the sum of the energies of all identied leptons, was required to be greater than $0.5 \quad E_{vis}$.

(B 6) The background from two-photon processes and "radiative return" events ($e^+e \; ! \; Z \;$, where the escapes down the beam pipe) was reduced by requiring that the polar angle of the missing momentum direction, $_{miss}$, satises $|\cos _{miss}| < 0.9$.

(B 7) To reduce further the total background from Standard Model lepton pair events, it was required that the energy sum of the two most energetic leptons be smaller than $0.75 \quad E_{vis}$.

To select nal states without missing energy, the following requirements were imposed:

(C 1) Events had to contain at least three identied isolated leptons each with a transverse momentum with respect to the beam axis greater than 1.5 GeV.

(C 2) It was also required that $0.65 < E_{vis}/\sqrt{s} < 2.0$.

(C 3) The total leptonic energy, dened as the sum of the energy of all identied leptons, was required to be greater than $0.65 \quad E_{vis}$. This distribution is shown in Figure 1 (c), after cuts (C 1) have been applied.

(C 4) To reduce the residual four-fermion background, pairs were formed with the four most energetic tracks, and the invariant mass was computed for each pair. Events were selected if one of the three possible pairings satises $|m_{i;j} \; m_{k;l}|/(m_{i;j} + m_{k;l}) < 0.4$, where $m_{i;j}$ is the invariant mass of the pair $(i;j)$. Only pairs with invariant mass $m_{i;j}$ greater than 20 GeV were used in the computation.

(C 5) To reduce further the total background from Standard Model lepton pair events, it was required that the energy sum of the two most energetic leptons be smaller than $0.75 \quad E_{vis}$.

The two analyses were then combined. Events passing either set of criteria were accepted as candidates. Detection eciencies range from 34% to 80% for direct sneutrino decays, and from 13% to 58% for indirect sneutrino decays, for sneutrino masses between 45 and 90 GeV. The expected background is estimated to be 2.5 events. There is one candidate event selected in the data.

5.4 Final States with Six Leptons plus Missing Energy

An analysis has been designed to select events with six charged leptons and missing energy in the final state. These topologies may for example result from indirect slepton decays with a coupling.

The following criteria were applied:

(D 1) To reduce the background from two-photon and di-lepton processes, it was required that $0.1 < E_{vis}/\sqrt{s} < 0.7$.

(D 2) The event longitudinal momentum was required to be smaller than $0.9 \cdot p_{vis}$, where p_{vis} is the event total momentum.

(D 3) The event transverse momentum calculated without the hadron calorimeter was required to be larger than $0.025 \cdot \sqrt{s}$. This distribution is shown in Figure 1(d) after cuts (D 1) and (D 2) have been applied.

(D 4) Events with less than five charged tracks with a transverse momentum with respect to the beam axis larger than 0.3 GeV were rejected.

(D 5) Events had to contain at least three well-identified isolated leptons; at least two of them with a transverse momentum with respect to the beam axis greater than 1.5 GeV, and the third one with a transverse momentum with respect to the beam axis greater than 0.3 GeV.

(D 6) The total leptonic energy, was required to be greater than $0.2 \cdot E_{vis}$.

Detection efficiencies range from 40% to 88% for indirect selectron decays, from 59% to 93% for indirect smuon decays and from 33% to 70% for indirect stau decays, for slepton masses between 45 and 90 GeV. The total background expectation is 1.7 events. There is one candidate event selected in the data.

5.5 Inefficiencies and Systematic Errors

Variations in the efficiencies were estimated with events generated with $m = 5$ GeV, as described in Section 3.

The inefficiency due to forward detector false vetoes caused by beam-related backgrounds or detector noise was estimated from a study of randomly triggered beam crossings to be 3.2%. The quoted efficiencies take this effect into account.

The systematic errors on the number of signal events expected that have been considered are: the statistical error on the determination of the efficiency from the Monte Carlo simulation (typically less than 2%); the systematic error on the integrated luminosity of 0.4%; the uncertainty due to the interpolation of the efficiencies, estimated to be 4.0% and the lepton identification uncertainty, estimated to be 2.4% for the muons, 3.9% for the electrons and 4.7% for the taus. The systematic error arising from the modelling of the variables used in the multi-lepton final state selections is smaller than the lepton identification uncertainties. The systematic error due to the trigger efficiency is negligible because of the high lepton transverse

momentum requirement. The total systematic error was calculated by summing in quadrature the individual errors and is incorporated into the limit calculation using the method described in Ref. [43].

The systematic error on the number of expected background events from SM processes has a negligible effect when computing limits.

6 Final States with Two Jets and Two Leptons

6.1 Electron and Muon Channels

In this section, the analysis for the selection of the final state of two electrons or two muons plus two jets and no missing energy is described. These final states may result from the direct decay of pair-produced stops via a ^{0} coupling. In contrast to the purely leptonic final states described in the previous section, the topologies searched for in this analysis involve hadronic jets; more stringent cuts are needed to obtain a purer lepton sample. Particles are considered as electrons or muons if they are either identified by the selection algorithms described in [39] and [40], or by an algorithm used for selecting semileptonic W decays, as described in [42].

Events were preselected by requiring the following criteria to be satisfied (the same criteria were also used for the analysis presented in Section 7):

The fraction of good tracks had to be greater than 0.2, to reduce beam-gas and beam-wall background events. Events with fewer than seven good charged tracks were not considered in order to reduce the background from Bhabha scattering. Events had to contain at least one identified electron or muon with a momentum greater than 3 GeV, to reduce the background from final states with low energy leptons (e or). To reduce background from two-photon processes, it was required that the visible energy normalised to the centre-of-mass energy, $R_{vis} = E_{vis}/\sqrt{s} > 0.3$.

The following cuts are then applied:

(E1) The visible energy had to be close to the centre-of-mass energy, $0.75 < R_{vis} < 1.25$. Figure 2(a) shows the visible energy distribution.

(E2) It was required that four jets be reconstructed using the Durham [44] algorithm, with $y_{34} > 0.001$, where y_{34} is the cut parameter between 3 and 4 jets. Both hadronic and leptonic objects are used in the jet reconstruction. Figure 2(b) shows the y_{34} distribution.

(E3) Events had to contain at least one pair of identified oppositely-charged lepton candidates of the same flavour.

(E4) To make use of the signal topology of two leptons and two jets, where a lepton and a jet stem from the same object, a five-constraint (5C) kinematic fit was performed for the two possible combinations of each lepton with each jet. The kinematic constraints are: the vector sum of all momenta has to be equal to zero, the total energy of all objects has to be equal to the centre-of-mass energy and the masses of the two reconstructed particles have to be equal. From the three most energetic leptons of the same flavour,

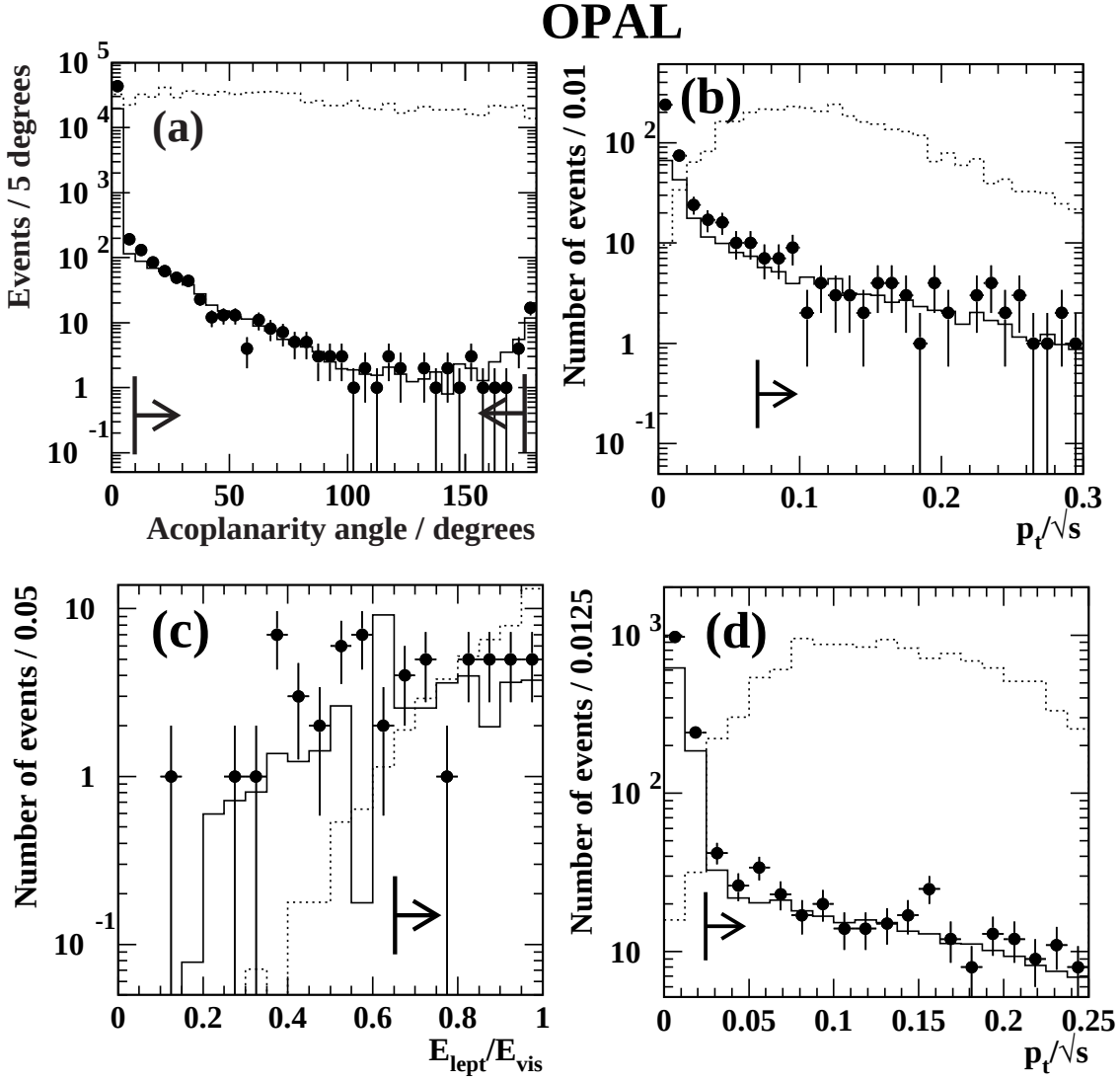

Figure 1: (a) Two lepton and missing energy search (Analysis A): Distribution of the acoplanarity angle. The dotted histogram shows signal Monte Carlo events for direct decays of e via $_{121}$ with $m_{e} = 70$ GeV. (b) Four lepton and missing energy search (Analysis B): Distribution of the event transverse momentum calculated without the hadron calorimeter. The dotted histogram shows signal Monte Carlo events for indirect decays of ~ with $m_{\sim} = 70$ GeV and for $_{233}$. (c) Four lepton and no missing energy search (Analysis C): Distribution of the sum of the energies of the identified leptons divided by the total visible energy. The dotted histogram shows signal Monte Carlo events for direct decays of ~ with $m_{\sim} = 70$ GeV and for $_{121}$. (d) Six lepton with missing energy search (Analysis D): Distribution of the event transverse momentum calculated without the hadron calorimeter. The dotted histogram shows signal Monte Carlo events for indirect decays of ~ with $m_{\sim} = 70$ GeV and for $_{233}$. Data are shown as points and the sum of all Monte Carlo background processes is shown as the solid line. The simulated signal events have arbitrary normalisation. The arrows point into the regions accepted by the cuts.

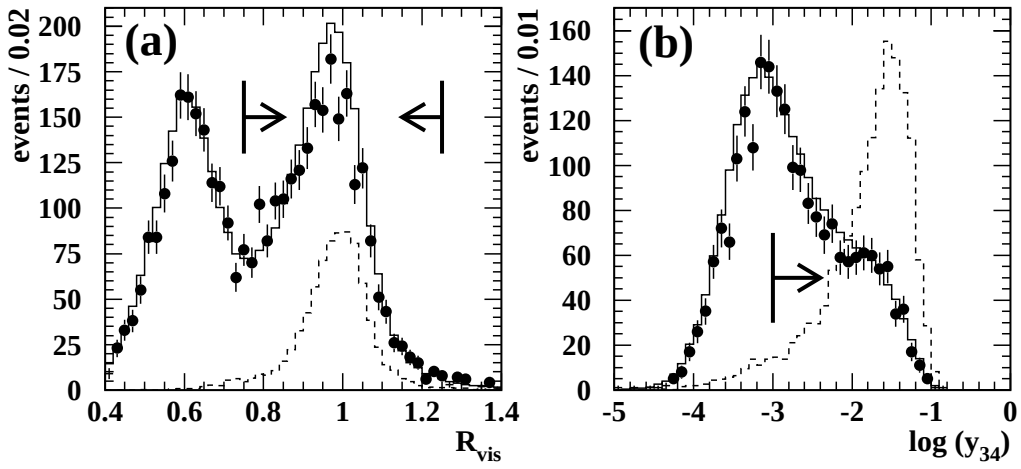

Figure 2: Stop search (Analysis E): (a) Visible energy R_{vis} after the preselection and (b) jet resolution y_{34} after cut (E1). Data are shown as points and the sum of all Monte Carlo background processes is shown as the solid line. The dashed histogram shows signal Monte Carlo events for direct decays of $\tilde{t}_1$ with $m_{\tilde{t}_1} = 85$ GeV and for $\tilde{\chi}^0_{ij3}$; $(i = 1;2)$. The scale of the signal MC is arbitrary. The arrows point into the regions accepted by the cuts.

the two most isolated[9] were selected and the rest of the event was reconstructed as two jets. The combination with the highest t probability was selected. The probability for the t, based on the ^{2}, was required to be larger than 0.01.

(E5) The momentum of the most energetic lepton had to be greater than 15 GeV and the momentum of the second most energetic lepton had to be greater than 10 GeV.

(E6) It was required that there be no charged track within 15 of the most energetic lepton candidate.

These cuts yield an efficiency of more than 50% for a stop mass of 65 GeV, which rises to approximately 65 % for masses above 85 GeV. No candidate event is selected in the data. The expected background is 0.9 events for final states with two electrons and 0.6 events for final states with two muons. The largest background results in both cases from WW events.

The following systematic errors have been considered:

1. The statistical error from the limited size of the Monte Carlo samples.
2. The error due to the interpolation of efficiencies for mass values between the generated stop masses, which was estimated to be less than 4% .
3. A 4% error due to the lepton identification for the electron and a 2% error for the muon channel.

[9] The most isolated lepton is the one with the largest angle to the closest track.

4. The fragmentation of the stop has been simulated using the fragmentation function from Peterson et al. with the parameter extrapolated from measurements of charm and bottom [45]. To check the model dependence of the fragmentation, it has also been performed using the function from Bowler [46]. No significant change in the efficiency due to the difference in the fragmentation function has been found. The difference is at most 0.5%, where a variation of the parameter of the c in the Peterson et al. scheme is included. This error on $_t$ is propagated from the error of $_b$ and the error on the b-quark mass as described in detail in Ref. [45].

5. The signal events have been produced for a zero mixing angle between the two stop eigenstates. The mixing angle describes the coupling between the stop and the Z^0, and therefore the energy distribution of the initial state radiation depends on this mixing angle. To check the dependence of the detection efficiency on this angle, events have been generated with $_t = 0.98$, where the stop decouples from the Z^0. The change in efficiency is less than 0.5% for the two extreme cases.

6. The Fermi motion of the spectator quark in the stop-hadron influences its measured mass. The Fermi motion has been increased from 220 MeV to 520 MeV and the efficiency changes by no more than 1%, which is taken as a systematic error.

7. The systematic error on the measured luminosity is 0.4%.

8. The systematic error due to the uncertainty in the trigger efficiency was estimated to be negligible, because of the requirement of at least seven good tracks.

The systematic error on the expected number of background events has been estimated to be less than 20% for all cases by varying the cut values by the experimental resolution.

6.2 Tau Channel

This section describes the analysis used to search for the final state consisting of two -leptons and two jets, which may result from the direct decay of a stop via a coupling ^{0}. The backgrounds come predominantly from $(Z/) \to q\bar{q}(\ )$ and SM four-fermion processes.

The selection begins with the identification of lepton candidates, identical to that in [47], using three algorithms designed to identify electronic, muonic and hadronic -lepton decays. An average of 2.3 candidates per signal event are identified. The original lepton direction is approximated by that of the visible decay products. The following requirements, similar to those described in Ref. [48] up to (F4), are then imposed:

(F1) Events are required to contain at least nine charged tracks, and must have at least two lepton candidates, including at least one pair where each has electric charge $|q| = 1$ and the charges sum to zero. Pairs not fulfilling these requirements are not considered further.

(F2) Events must have no more than a total of 20 GeV of energy deposited in the forward detector, gamma catcher, and silicon-tungsten calorimeter; a missing momentum vector satisfying $|\cos _{miss}| < 0.97$, a total transverse momentum of at least 2% of $\sqrt{s}$, and a scalar sum of all track and cluster transverse momenta larger than 40 GeV.

(F 3) Events must contain at least three jets reconstructed using the cone algorithm as in [47][10], and no energetic isolated photons[11].

(F 4) Events must contain no track or cluster with energy exceeding $0.3\sqrt{s}$.

For events surviving these requirements, the hadronic part of the event corresponding to each surviving lepton candidate pair, composed of those tracks and clusters not having been identified as belonging to the pair (henceforth referred to as the "rest of the event" or RoE), is then split into two jets using the Durham [44] algorithm. Two pairings between the two candidates and the jets are possible. The invariant masses m_j of the two resulting -jet systems within each pairing are then calculated using only the lepton and jet momentum directions and requiring energy and momentum conservation. The pairing scheme with the smaller difference between m_{j1} and m_{j2} is then chosen. In order for a candidate pair to be considered further, the following requirements on m_{j1} and m_{j2} are imposed, consistent with the hypothesis of the decay of two heavy objects of identical mass:

(F 5) Both m_{j1} and m_{j2} must be at least 30 GeV.

(F 6) The difference in invariant masses must be no more than 30% of their sum, i.e. $|m_{j1} - m_{j2}|/|m_{j1} + m_{j2}| < 0.3$.

The distribution of $|m_{j1} - m_{j2}|/|m_{j1} + m_{j2}|$ is shown in Fig. 3 (a) for the data, the backgrounds, and for a signal sample with $m_{\tilde{t}} = 75$ GeV. The resolution on m_j is typically below 5 GeV, except very close to the kinematic limit.

A likelihood method similar to that described in [5] is then applied to those events satisfying the above requirements, in order to select a final candidate pair for each event from those surviving, and to suppress further the remaining background.

Distributions of two of the input variables as well as that of L are shown in Figures 3 (b) to (d). In each event, the -candidate pair with the highest value of L is chosen, and the following requirement is then made:

(F 7) $L > 0.93$

Two events survive the selection while the background, almost all from four-fermion processes, is estimated to be 2.07 events for an integrated luminosity of 55.8 pb^{-1}. The reconstructed -jet masses are 78.9 and 87.9 GeV for the first selected event and 71.7 and 67.2 GeV for the second one.

The detection efficiencies for stop masses between 55 and 90 GeV range from 30 to 40%, while that for 45 GeV is approximately 22%.

These efficiencies are affected by the following relative uncertainties: Monte Carlo statistics, typically 2.5 to 3.5%; uncertainty in the tau-lepton preselection efficiency, 1.2%; uncertainty in the modelling of the other preselection variables, 2.0%; uncertainties in the modelling of the

[10] Here, single electrons and muons from lepton decays are allowed to be recognised as low-multiplicity "jets".

[11] An energetic isolated photon is defined as an electromagnetic cluster with energy larger than 15 GeV and no track within a cone of 30 half-angle.

likelihood input variables, 10.0% ; uncertainties in the modelling of fragmentation and hadronisation, 6.0% ; and uncertainty on the integrated luminosity, 0.5% [49]. Taking these uncertainties as independent and adding them in quadrature results in a total relative systematic uncertainty of 12.3% The systematic uncertainty in the number of expected background events was estimated to be 18% .

7 Final States with more than Two Jets and at Least two Charged Leptons

7.1 Indirect Selectron and Smuon Decays

This section describes the event selection for final states from the indirect decay of selectrons and smuons via the coupling ^{0}. The final state consists of two leptons of the same flavour from the sleptons plus the decay products of the two $\tilde{\chi}_1^0$'s. These will be two jets plus a neutral or charged lepton for each $\tilde{\chi}_1^0$. This results in seven different final states for each slepton flavour, as shown in Table 3. Electrons and muons are identified as described in Section 6.1. To identify taus in the final states an Artificial Neural Net based on tracks [50] is used, rather than the selection presented in Section 6.2 designed specifically for events with two 's.

The preselection is the same as described in Section 6. The selection cuts are as follows:

(G 1) A cut on the visible energy scaled by the centre-of-mass energy in the range $0.5 < E_{vis}/\sqrt{s} < 1.2$, depending on the expected number of neutrinos, is applied. In addition a cut on the angle of the missing momentum with respect to the beam direction at $|\cos| < 0.95$ is performed, if some missing momentum is expected.

(G 2) The jets in the event have been reconstructed using the Durham algorithm. The jet resolution y_{45} at which the number of jets changes from 4 to 5 jets, is required to be greater than 0.002. This cut takes into account the high multiplicity of the signal events.

(G 3) To reduce the background from W pair production for events with missing momentum, a single-constraint kinematic fit has been performed. The inputs to the fit are the momenta of the lepton and the neutrino, taking the missing momentum to be the momentum of the neutrino, and the rest of the event reconstructed into 2 jets. The lepton is taken to be the most energetic muon or electron in the case of smuon or selectron production, respectively. The invariant mass is calculated (a) for the lepton and the neutrino system and (b) for the two jet system, letting the masses of both systems be independent. The reconstructed mass of at least one system has to be outside a mass window of $70\ \mathrm{GeV} < m < 90\ \mathrm{GeV}$, or the probability for the fit has to be less than 0.01.

(G 4) For the topologies with no charged lepton from the $\tilde{\chi}_1^0$ decay, the background from W pair production is reduced further by a kinematic fit on the invariant mass of two pairs of jets, when reconstructing the whole event into 4 jets. This kinematic fit assumes energy and momentum conservation and the same mass for both jet pairs. From the three possible jet pairings, the one with the highest fit probability is chosen. The reconstructed mass of the jet pairs has to be outside a mass window of $70\ \mathrm{GeV} < m < 90\ \mathrm{GeV}$, or the probability for the fit has to be less than 0.01.

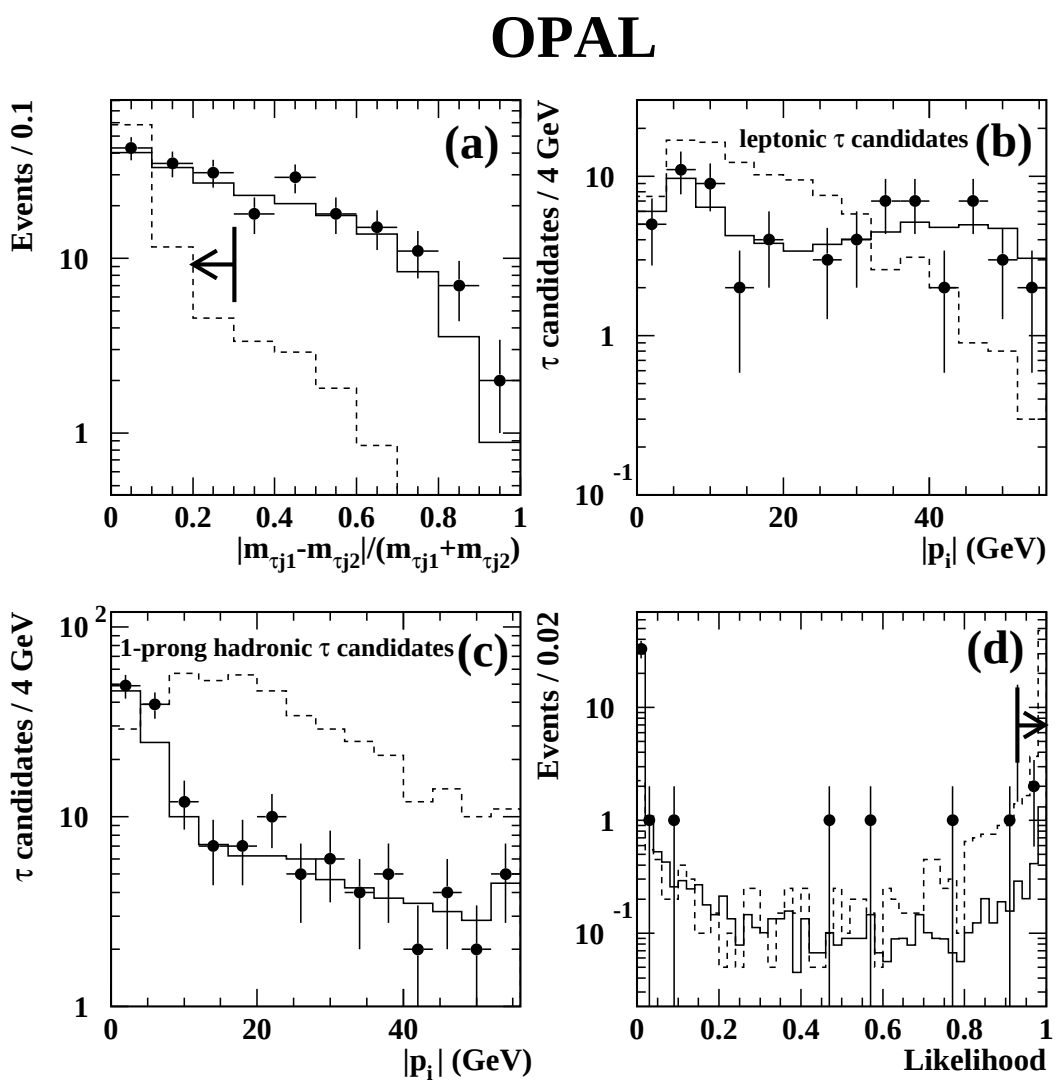

Figure 3: Search for jets plus at least two leptons (Analysis F): Distributions of relevant quantities for data (points), estimated Standard Model background (full histogram) normalised to the integrated luminosity of the data, and a simulated signal (dashed histogram, arbitrary normalisation) corresponding to $m_{\tilde{t}_1} = 75$ GeV (direct decay). (a) Distribution of the difference in invariant mass of the tau-jet system scaled by their sum after cut (F2); events to the left of the arrow indicating the cut position are accepted. Figures (b) and (c) show the difference in the distributions of the same likelihood input variable for two different categories of candidates, after cut (F4): (b) The momentum of leptonic candidates; (c) the momentum of 1-prong hadronic candidates. The likelihood distribution is shown in (d) after cut (F6). The arrows point into the regions accepted by the cuts.

(G 5) At least two leptons of the avour of the slepton have to be identi ed. To have sensitivity also to small mass di erences between the slepton and the $\tilde{\chi}_1^0$, the required momentum has to be greater than 4 GeV for both muons in the smuon case and the required energy greater than 4 GeV and 3 GeV for the two electrons in the selectron case, respectively.

(G 6) In addition to the leptons required in (G 5), also the leptons from the $\tilde{\chi}_1^0$ decay have to be identi ed. If two additional charged leptons are expected, both have to be identi ed, if they have a di erent avour than the slepton. If two taus are expected, only one, being di erent from the leptons in cut (G 5), has to be identi ed. If a total of four leptons of the same avour is expected, including those in cut (G 5), only three of them have to be identi ed.

If only one additional lepton is expected, it has to be identi ed.

The energy or momentum of the most energetic lepton has to be above a cut value varying between 8 and 15 GeV, depending on the topology. If a total of four leptons is required, for the second most energetic an energy or momentum larger than a cut value varying between 3 GeV and 4 GeV, depending on the topology, is required.

(G 7) To make use of the isolation of the leptons in the signal, one or two of the identi ed leptons, depending on the expected topology, are required to be isolated. The isolation criterion is that there be no charged track within a cone of half opening angle , such that $|\cos| = 0.99$, around the track of the lepton.

These selections give e ciencies between 45 and 85% for nal states without taus, and around 30% for nal states with taus, all for slepton masses greater than 70 GeV. The expected backgrounds and the numbers of events observed for each nal state are shown in Table 3.

System atic Errors

For the lepton identi cation, a system atic error of 4% was estim ated for the electrons, 3% for the muons and 3% for the taus. For the interpolation of the e ciency between the generated mass points, a system atic error of 4% has been assigned. From the studies on the fragm entation in Section 6 the system atic error for this analysis is estim ated to be less than 1%. The system atic error on the measured lum inosity is 0.4%. The system atic error due to the uncertainty in the trigger e ciency is negligible, because of the requirem ent of at least seven good tracks. The statistical error on the determ ination of the e ciency from the MC samples has also been treated as a system atic error. The system atic error on the expected number of background events has been estim ated to be less than 20% for all cases.

7.2 Stau Indirect Decays

If requirements (F 5) and (F 6) described in Section 6.2 are suppressed, then the same analysis as that for the stop search in the tau channel can be used to search for the indirect decay of staus via the coupling ^{0}, where now the nal state consists of two leptons plus four jets and two additional leptons. In this case, the reference distributions are regenerated in light of the di erent topology of this signal, and the m inim um required value of the resulting likelihood discrim inant L (cf. (F 7)) is relaxed to 0.9. No events survive the selection while the

Final State	Selected Events	Tot. bkg MC
$\tilde{}^{+}\tilde{}$!		
$^{+}$ eqqeqq	2	0.69
$^{+}$ qq qq	1	0.67
$^{+}$ qq qq	1	1.10
$^{+}$ eqq qq	3	1.05
$^{+}$ qq qq	1	0.95
$^{+}$ qq qq	0	0.58
$^{+}$ qq qq	0	0.91
$e^{+}e$!		
$e^{+}e$ eqqeqq	1	0.29
$e^{+}e$ qq qq	1	0.37
$e^{+}e$ qq qq	3	1.09
$e^{+}e$ eqq qq	1	0.52
$e^{+}e$ qq qq	2	1.10
$e^{+}e$ qq qq	3	0.81
$e^{+}e$ qq qq	0	1.13

Table 3: Number of events remaining after the selection cuts and the expected backgrounds from all Standard Model processes. The main contribution to the total background comes from $W^{+}W$ leptonic decays (4-fermion processes); multi-hadronic events contribute up to 30% and other processes are negligible.

background expectation rises slightly to 2.27 events. The detection efficiencies range from 12% for final states with two taus, four quarks plus missing energy and $m_{\tilde{}} = 45$ GeV, to 54% for final states with two taus, four quarks plus two electrons and $m_{\tilde{}} = 70$ GeV. The systematic uncertainties are evaluated in the same way as for the stop search as described in Section 6.2, and are similar in magnitude.

8 Final States with Four Jets plus Missing Energy

Indirect decays of sneutrinos via ^{0} coupling can lead to final states with four jets and large missing energy due to the four undetected neutrinos. The dominant backgrounds come from four-fermion processes and radiative or mis-measured two-fermion events. The selection procedure is described below:

(H 0) The event has to be classified as a multi-hadron final-state as described in [51].

(H 1) The visible energy of the event is required to be less than $0.75\sqrt{s}$.

(H 2) To reject two-photon and radiative two-fermion events the transverse momentum should be larger than 10 GeV, the total energy measured in the forward calorimeter, gamma-catcher and silicon tungsten calorimeter should be less than 20 GeV, and the missing momentum should not point along the beam direction ($|\cos_{miss}| < 0.96$).

(H 3) The events are forced into four jets using the Durham jet-finding algorithm, and rejected if the jet resolution parameter y_{34} is less than 0.0008.

(H 4) An additional cut is applied against semi-leptonic four-fermion events, vetoing on isolated leptons being present in the event. The lepton identification is based on an Artificial Neural Network routine (ANN) [50], which was originally designed to identify tau leptons but is efficient for electrons and muons, as well. If at least one lepton candidate is found, with ANN output larger than 0.97, the event is rejected.

(H 5) Finally, a likelihood selection is employed to classify the remaining events as two-fermion, four-fermion or signal processes. The method and the likelihood variables are described in [5], with the restriction that the minimum number of charged tracks and the minimum number of electromagnetic clusters in a jet are replaced by the aplanarity of the event [52]. The event is rejected if its likelihood output is less than 0.9.

Figure 4 shows experimental plots for the data, the estimated background and simulated signal events.

After all cuts, 5 events are selected in the data sample, while 8.17 0.31 1.32 events are expected from Standard Model processes, of which 75% originate from four-fermion processes. The signal detection efficiency varies between 5% and 34% for sneutrino masses between 45 – 90 GeV for $^{0}_{121}$ and $^{0}_{123}$ couplings if the mass difference is one half of the sneutrino mass. For a small mass difference (5 GeV), the efficiency is more than doubled.

The small efficiency for light sneutrino masses is the result of initial-state radiation and the larger boost of the particles, which make the event similar to the QCD two-fermion background.

The expected signal rates are affected by the following uncertainties: Monte Carlo statistics, 3.3 – 13.9% ; statistical and systematic uncertainties on the luminosity measurement, 0.3 and 0.4% ; uncertainties on modelling of the kinematic variables, 6.7% ; and on the lepton veto, 1.0% .

The background estimate has the following errors: Monte Carlo statistics, 3.7% ; modelling of the hadronisation process estimated by comparing different event generators, 5.3% ; uncertainty on the lepton veto, 1% ; and modelling of the kinematic variables, 14.9% .

The inefficiency due to the forward energy veto is found to be 1.8% .

9 Final States with Four Jets without Missing Energy

Direct decays of sleptons (squarks) via ^{0} (^{00}) coupling can result in final states with four well-separated, high multiplicity hadronic jets and large visible energy. The background comes from $qq(\ )$ events with hard gluon emission and four-fermion processes, predominantly $W^{+}W$! $qqqq$.

The analysis closely follows our published selection for $H^{+}H$! $qqqq$ [50]. First, well-defined four-jet events are selected; then a set of variables are combined using a likelihood technique.

The preselection consists of the following steps:

(I0) The event has to be classified as a multi-hadron final-state as described in [51].

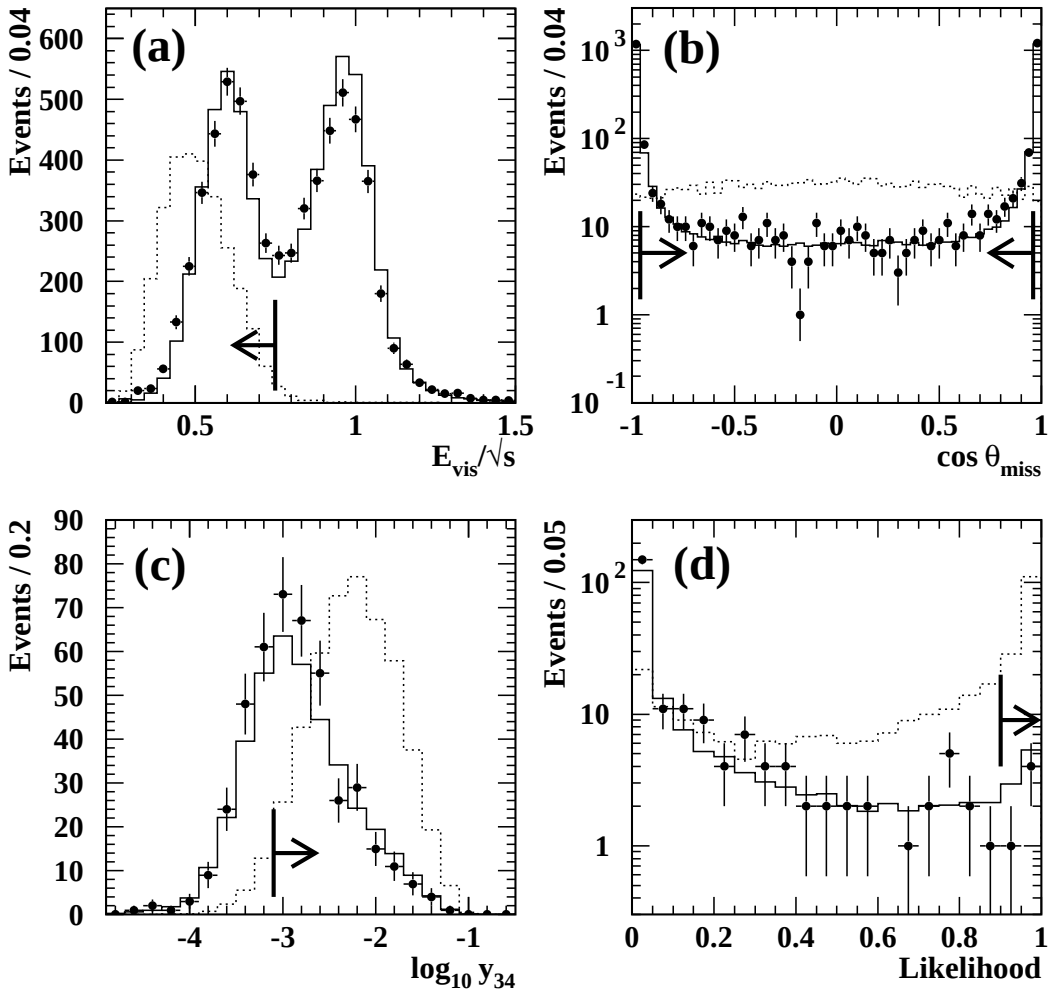

Figure 4: Four jets plus missing energy search (Analysis H): Distributions for data (points), for the estimated Standard Model background (full histogram) and for a sum of simulated signals (dotted histogram). Figure (a) shows the visible energy, E_{vis}, divided by the centre of mass energy, $\sqrt{s}$, for multi-hadron events after cut (H0). In Figure (b) the distribution of the cosine of the polar angle of the missing momentum vector is plotted after cut (H1). In Figure (c) the logarithm of the jet resolution, y_{34}, at which the number of reconstructed jets changes between 4 and 3, is shown after cut (H2) has been applied. Figure (d) shows the final selection using the likelihood output. The arrows indicate the accepted regions in each plot. The Standard Model background is normalised to the integrated luminosity of the data, while the normalisation of the signal distribution is arbitrary.

(I1) To reduce the radiative two-fermion background, the effective centre-of-mass energy of the event, $\sqrt{s'}$ [53], is required to be greater than 150 GeV.

(I2) To ensure that the events are well-contained, the visible energy should be greater than $0.7\sqrt{s}$.

(I3) The events are forced into four jets using the Durham jet-finding algorithm, and rejected if the jet resolution parameter y_{34} is less than 0.0025. Moreover, all jets must contain at least one charged particle.

(I4) A four-constraint kinematic fit, applied to the jet four-momenta requiring energy and momentum conservation (4C-fit), should yield a χ^2-probability larger than 10^{-5}.

(I5) To test the compatibility with pair-produced equal mass objects and to obtain the best possible di-jet mass resolution, the jet four-momenta are refitted requiring energy and momentum conservation and equal di-jet masses (5C-fit). The event is kept if at least one of the three di-jet combinations has a χ^2-probability larger than 10^{-5}.

To separate the signal from the background events surviving the above selection a likelihood technique is applied. Three event classes are defined: signal, two-fermion and four-fermion.

9.1 Sleptons

We have used the $H^+H^- \to$ cscs MC samples to produce the signal reference histograms. This is possible because of the similarities between charged Higgs and smuon, stau, muon- and tau-sneutrino decays. Since selectrons and electron-sneutrinos can also be produced in t-channel-exchange processes, their event properties (especially the angular distributions) are different, and we have used dedicated MC samples with λ'_{121} and λ'_{123} couplings to produce these reference histograms.

The following variables were used as input to the likelihood calculation:
the cosine of the polar angle of the thrust axis;
the cosine of the smallest jet-jet angle;
the difference between the largest and smallest jet energy after the 4C-fit;
the smallest di-jet mass difference after the 4C-fit;
the cosine of the di-jet production angle multiplied by the sum of the jet charges for the combination with the highest χ^2-probability given by the 5C-fit.

Events were accepted if their likelihood output was larger than 0.5, 0.55 and 0.6 for selectrons, electron-sneutrinos and other sleptons, respectively.

The numbers of selected data and expected background events are listed in Table 4 for the different selections. Since the background is dominated by W^+W^- production (82–87%), the mass distributions are peaked around the $W^\pm$ boson mass. No excess (unexpected accumulation) was observed in the data. Figure 5a shows, as an example, the mass distribution of the selected events for the data, the estimated background and simulated selectron events.

The di-jet mass resolution using the 5C-fit is 0.6–1.6 GeV, depending on the sparticle mass and decay. Events in a 2σ mass window around the test mass were selected. The efficiencies vary between 11.3% and 34.3% within such a mass window for sparticle masses between 50 and 75 GeV, depending on the sparticle mass and decay.

	Data	Background
Preselection	454	445.4 2.3
Selectron	55	55.4 0.8
Electron-sneutrino	41	49.1 0.7
Other sleptons	50	48.8 0.7
Squarks	7	8.8 0.3

Table 4: The numbers of selected data and expected background events in the four-jet channel after the preselection and at the end of the different selections. Only the statistical error is indicated.

The signal detection efficiency is subject to the following inefficiencies and systematic errors: the statistical error due to the limited number of Monte Carlo events, 4.4{17.7% ; the uncertainty on modelling the kinematic variables used in the analysis, 3% ; and additionally for the smuon, muon-sneutrino, stau and tau-sneutrino selection, the inefficiency due to the differences between the slepton and the charged Higgs boson simulation, 0{12% .

The background estimate has the following uncertainties: the statistical error due to the limited number of Monte Carlo events, 1.5% ; the statistical and systematic error on the luminosity measurement, 0.3 and 0.4% ; the uncertainty on modelling the SM background processes, estimated by comparing different event generators, 2% ; and the kinematic variables used in the analysis, 4.9% .

9.2 Squarks

Squarks are expected to hadronize resulting in a final state with six jets, from which the two spectator jets have small energy, at least for heavy squarks, and therefore it is still possible to reconstruct the squark pair events into four jets.

To produce the signal reference histograms, we have used dedicated squark samples generated by SUSYGEN with $^{00}_{121}$ and $^{00}_{123}$ couplings. Since jets originating from squark decays are narrower than the ones coming from Standard Model sources, in addition to the five input variables used in the slepton searches, two new variables are introduced:

the smallest boosted jet thrust;
the highest jet mass.

The events are rejected if their likelihood output is less than 0.95.

Figures 5b-d show experimental plots for the data, the estimated background and simulated signal events. The numbers of selected data and expected background events are listed in Table 4. Since the background is dominated by W^+W^- production (93.3%), the mass distribution is peaked around the W^- boson mass. No unexpected accumulation of events is observed in the data.

The di-jet mass resolution using the 5C kinematic fit is 0.45{1.2 GeV, depending on the squark mass and decay. A systematic shift of the reconstructed mass (up to +2.2 GeV for squark masses of 45 GeV) is observed, which is taken into account when applying the 2 mass

window. The signal detection efficiencies within the mass windows vary between 14.1% and 29.8% for squark masses of 45–90 GeV.

The signal detection efficiency is subject to the following inefficiencies and systematic errors: the statistical error due to the limited number of Monte Carlo events, 4.9–7.8%; and the uncertainty on modelling the kinematic variables used in the analysis, 13.2%.

The effect of different fragmentation and hadronization models has been tested comparing SUSYGEN and a special stop generator [54] used in OPAL stop searches [23]. It was found that SUSYGEN produces wider (more SM-like) jets, and our efficiency would be more than a factor of two higher for events generated by the stop generator. Thus our efficiency estimates using SUSYGEN are considered to be conservative.

The background estimate has the following uncertainties: the statistical error due to the limited number of Monte Carlo events, 3.6%; the statistical and systematic error on the luminosity measurement, 0.3 and 0.4%; the uncertainty on modelling the SM background processes, estimated by comparing different event generators, 20.4%; and the kinematic variables used in the analysis, 23.8%.

The result of the slepton and squark analyses is combined with previous searches performed at $\sqrt{s} = 130$–172 GeV for pair-produced, equal mass scalar particles (charged Higgs bosons) [55] in order to increase the sensitivity for low mass sleptons and squarks. These previous searches are assumed to be equally efficient for slepton, squark and charged Higgs search. This hypothesis has been tested using slepton (squark) Monte Carlo samples generated at $\sqrt{s} = 172$ GeV for several λ' (λ'') couplings with sparticle masses of 45, 55 and 70 GeV. The efficiencies are found to be consistent within the statistical errors except for the squark samples, where a relative 20% increase in the efficiency is observed. Conservatively, this gain is not taken into account.

10 Interpretation

No significant excess of events in the data with respect to the expected background has been observed for all analyses listed in Table 1. Production cross-section and mass limits have therefore been computed. These limits also take into account indirect limits obtained from the study of the Z^0 width at LEP1 and therefore concern only sparticle masses above 45 GeV.

Two approaches are used to present sfermion production limits. In the first one, upper limits on production cross-sections as functions of the sfermion masses are calculated with minimal model assumptions. These upper limits in general do not depend on the details of SUSY models, except for the assumptions that the sparticles are pair-produced and that only one λ-like coupling at a time is nonzero, as stated in Section 1. In the second approach, limits on the sfermion masses were calculated in the framework of the Constrained MSSM where mass limits are derived using the following parameters: m_0, the common sfermion mass at the GUT scale; M_2, the SU(2) gaugino mass parameter at electroweak scales[12]; μ, the mixing parameter of the two Higgs doublets and $\tan\beta = v_2/v_1$, the ratio of the vacuum expectation values for the two Higgs doublets. For the indirect sfermion decays, we have used the branching ratios for the decay $\tilde{f} \to f\tilde{\chi}^0_1$ predicted by the MSSM, and we have conservatively assumed no experimental sensitivity to any other decay mode. The branching ratio for direct decay is always treated as

[12] We assume that M_1, the U(1) gaugino mass at electroweak scales, is related to M_2 by the usual gauge unification condition: $M_1 = \frac{5}{3}\tan^2\theta_W M_2$.

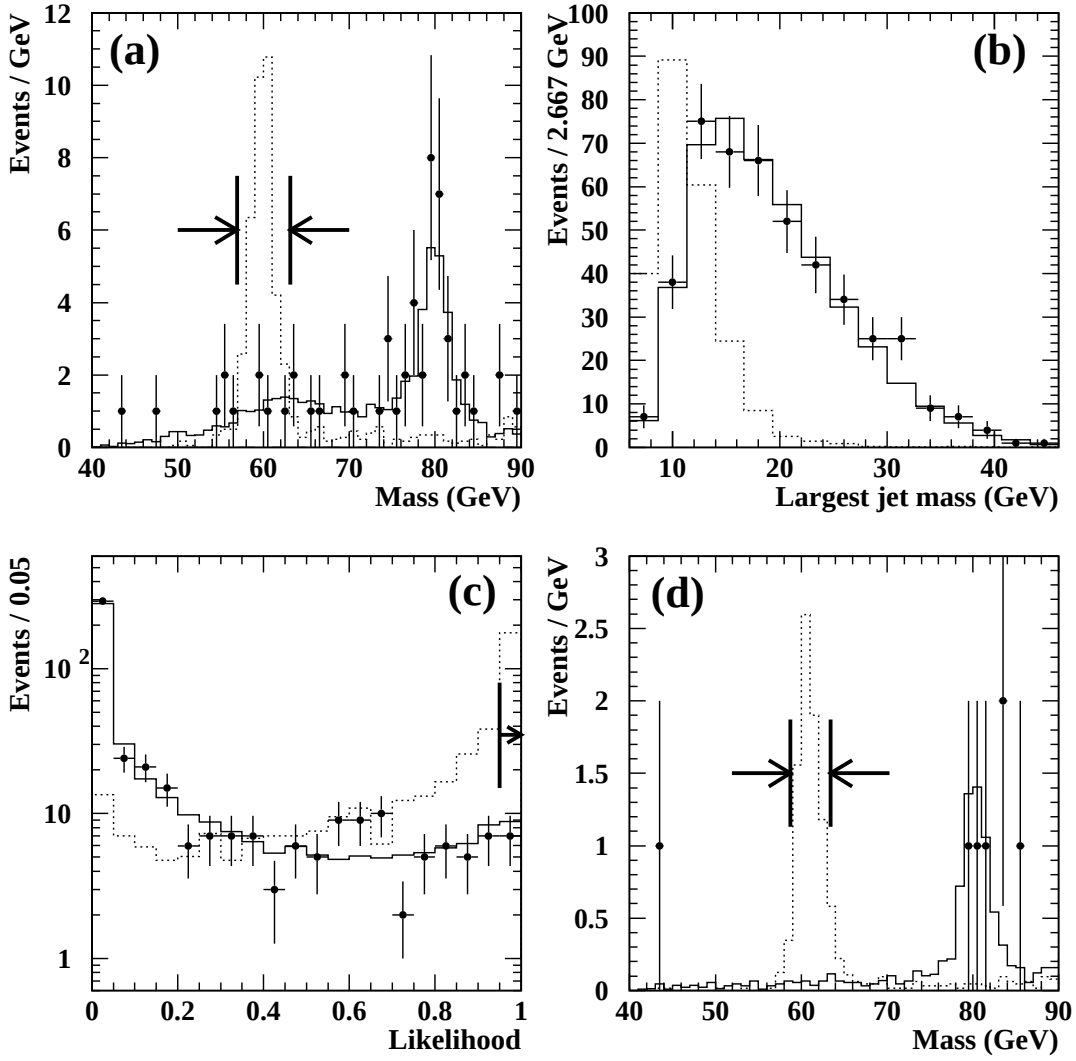

Figure 5: Four jets search (Analysis I): Distributions for data (points), for the estimated SM background (full histogram) and for simulated signal events (dotted histogram). Selectron search: Figure (a) shows the mass distribution of selected events. The mass window for a 60 GeV selectron is indicated by arrows. Squark search: In Figure (b) one of the likelihood reference distributions, the largest jet mass, is plotted. In Figure (c) the selection on the likelihood output can be seen. In Figure (d) the mass distribution of selected events is plotted. The arrows indicate the mass window for a 60 GeV squark. The SM background is normalised to the integrated luminosity of the data, while the normalisation of the signal distribution is arbitrary.

equal to 1, as we allow only one coupling to be different from zero at a time. The MSSM mass exclusion plots presented in the following sections are computed for tan = 1.5 and = { 200 GeV. This choice of parameters is rather conservative as sfermion production cross-sections generally increase for larger values of tan or j j.

In the indirect decay of a sfermion, f̃ ! f $\tilde{\chi}_1^0$, via a ^{0} coupling, the $\tilde{\chi}_1^0$ decays either as:

$$\tilde{\chi}_1^0 \to \nu_i u_j \bar{d}_k ; \quad \tilde{\chi}_1^0 \to \nu_i^+ \bar{u}_j d_k ; \tag{2}$$

or as:

$$\tilde{\chi}_1^0 \to {}_i d_j \bar{d}_k ; \quad \tilde{\chi}_1^0 \to \bar{}_i \bar{d}_j d_k \tag{3}$$

This leads to nal states with two fermions from the sfermion decay plus the $\tilde{\chi}_1^0$ decay products:

1. Four jets and two charged leptons if both $\tilde{\chi}_1^0$ decay via (2)
2. Four jets and missing energy if both $\tilde{\chi}_1^0$ decay via (3)
3. Four jets, one charged lepton and one neutrino if one $\tilde{\chi}_1^0$ decays via (2) and the other via (3).

The relative branching ratios of the neutralino into a nal state with a charged or a neutral lepton depends on the mass of the sneutrinos, the mass of the sleptons and on the components of the gaugino (Wino or Higgsino). To avoid a dependence of the results on the MSSM parameters, the branching ratio of $\tilde{\chi}_1^0$ to charged leptons and jets (2) was varied between 0 and 1. The branching ratio of $\tilde{\chi}_1^0$ to neutrinos and jets (3) was varied accordingly between 1 and 0. The combination of these two branching ratios xes the branching ratio for one $\tilde{\chi}_1^0$ decaying via (2) and the other via (3). A likelihood ratio method [56] was used to determine an upper limit for the cross-section. This method combines the individual analyses looking for the different nal states possible for one given ^{0} coupling and assigns greater weight to those with a higher expected sensitivity, taking into account the expected number of background events. This results in a cross-section limit as a function of the branching ratio and the sfermion mass. By taking the worst limit at each sfermion mass, a limit independent of the branching ratio is determined. For the direct decays, the nal states are fully determined by the indices of the coupling considered.

In the following sections, cross-sections limits are shown for the various direct and indirect decays studied in this paper, see Table 1. In each cross-section plot, only the curve corresponding to the worst cross-section limit is shown amongst all possible cross-section limits resulting from the couplings considered. The coupling yielding the worst cross-section limit is indicated in each plot. Generally, the best excluded cross-section comes from nal states with a maximum number of muons and no taus, while the worst results come from nal states with many taus, due to their lower detection eciency.

In the MSSM framework, the exclusion regions for the indirect decays are valid for m = m . m $_{\tilde{\chi}_1^0}$ 5 GeV except for the indirect decays of staus via ^{0} which are valid for m = m . m $_{\tilde{\chi}_1^0}$ 22:5 GeV. In this particular case there is not enough sensitivity to place limits in the small m region. The exclusion region for the direct decays is independent of m .

All limits presented here are quoted at the 95% C.L. The inefficiencies due to different angular distributions (possible for selectron or electron sneutrino pair production via the t-channel) of produced sfermions and decay products were estimated for five different MSSM parameter sets, representing different neutralino field contents (gaugino/higgsino) and couplings, and calculated separately for each analysis. The selection efficiencies may vary by up to 10%. In interpreting the results, a conservative approach was adopted by choosing the lowest efficiencies in the limit calculation. The systematic and the statistical errors were added in quadrature and then subtracted when using the number of background events.

10.1 Selectron Limits

Figure 6 shows upper limits on the cross-sections of pair-produced $\tilde{e}$ followed by a decay via a λ coupling: for (a) the direct decay of a right-handed $\tilde{e}_R$, (b) the direct decay of a left-handed $\tilde{e}_L$ and (c) the indirect decay of a $\tilde{e}_R$. The production cross-section for left-handed sfermion is always larger that for right-handed sfermions, therefore we have conservatively quoted results for right-handed sfermions only. For all cases, the worst upper limit on the cross-section is 0.36 pb.

Figure 7 shows upper limits on the cross-sections of pair-produced $\tilde{e}$ followed by a decay via a λ' coupling: for (a) the indirect decay of a $\tilde{e}_R$ in the electron channel, (b) the indirect decay of a $\tilde{e}_R$ in the muon channel and (c) the indirect decay of a $\tilde{e}_R$ in the tau channel. For all cases, the weakest upper limit on the cross-section is 2.5 pb.

Figure 8 shows upper limits on the cross-sections of pair-produced $\tilde{e}$ directly decaying via a λ' coupling to a four-jet final state. The peak structure visible in the figure at approximately the mass of the W-boson comes from irreducible background due to WW pair-production.

In the MSSM, the $\tilde{e}$ pair-production cross-section is enhanced by the presence of the t-channel diagram. Figure 9(a) shows the 95% C.L. exclusion limits for right-handed selectrons decaying directly or indirectly via a λ coupling. In the region where the $\tilde{\chi}_1^0$ is heavier than the $\tilde{e}$, only direct decays are possible. When the $\tilde{\chi}_1^0$ is lighter than the $\tilde{e}$, the indirect decays are expected to be dominant. For indirect decays via a λ coupling, a right-handed selectron with a mass smaller than 84 GeV is excluded at the 95% C.L. in the case of a low-mass $\tilde{\chi}_1^0$. For direct decays via a λ coupling, a right-handed selectron with a mass smaller than 84 GeV is excluded at the 95% C.L. Figure 9 (b) shows the 95% C.L. exclusion limits for selectrons decaying via a λ' coupling. The exclusion refers to right-handed selectrons for the indirect decays and to left-handed selectrons for direct decays. In the case of indirect decay, a right-handed selectron with a mass smaller than 72 GeV is excluded at the 95% C.L. in the case of a low-mass $\tilde{\chi}_1^0$ and a left-handed selectron with a mass smaller than 76 GeV is excluded in the case of direct decays.

10.2 Smuon Limits

Figures 10 and 11 show upper limits on the cross-sections for pair-produced $\tilde{\nu}$. The weakest upper limit on the cross-section is 0.30 pb for the λ couplings and 0.48 pb for the λ' couplings.

Figure 12 shows upper limits on the cross-sections of pair produced $\tilde{\nu}$ directly decaying via a λ' coupling to a four-jet final state.

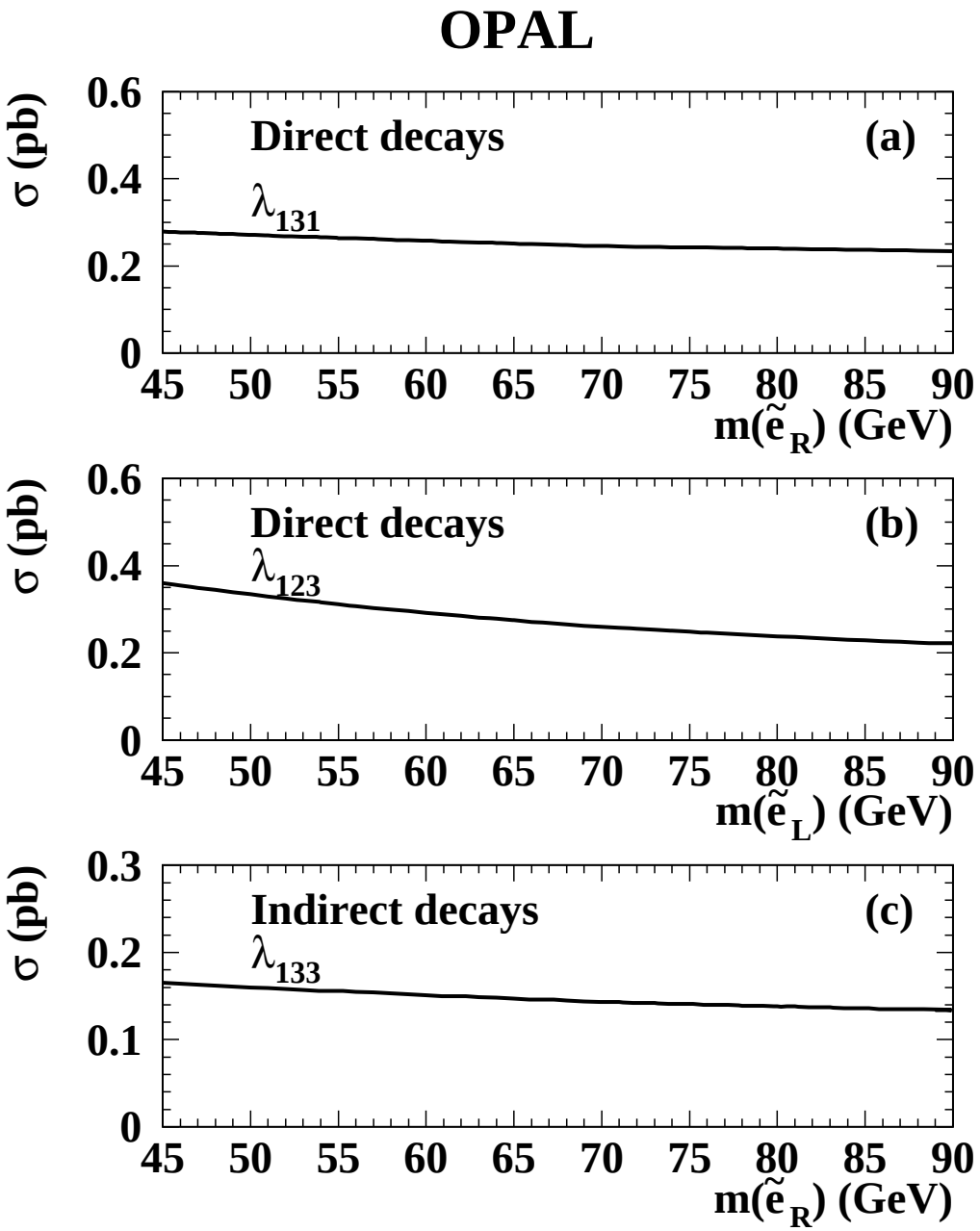

Figure 6: Selectron decays via a coupling: Upper limits at the 95% C.L. on the pair-production cross-sections for (a) the direct decay of a right-handed e_R, (b) the direct decay of a left-handed e_L and (c) the indirect decay of a e_R. Only the worst limit curve is shown and the corresponding to it is indicated.

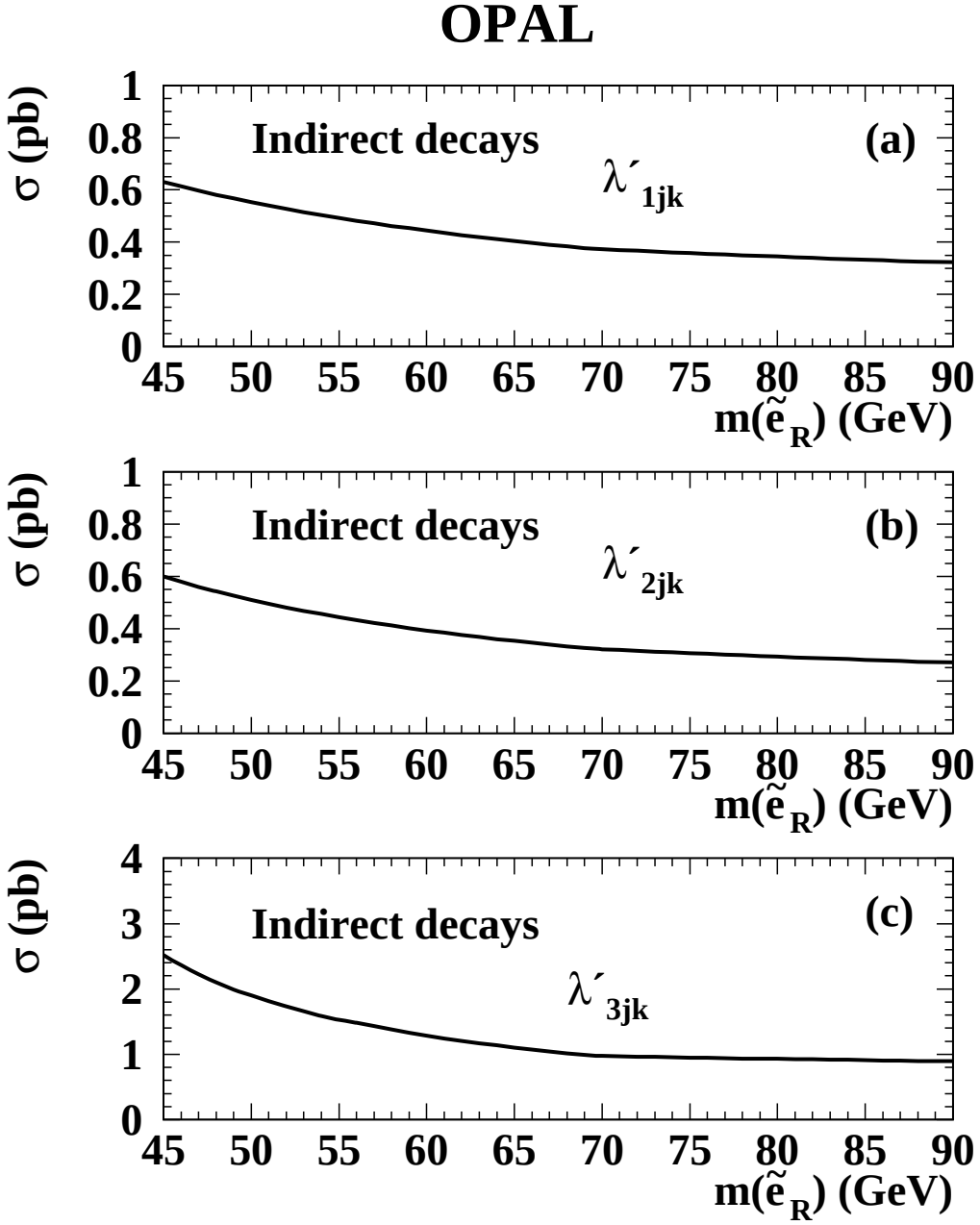

Figure 7: Indirect selectron decays via a ^{0} coupling: Upper limits at the 95% C.L. on the pair-production cross-sections for (a) the indirect decay of a e_R in the electron channel, (b) the indirect decay of a e_R in the muon channel and (c) the indirect decay of a e_R in the tau channel.

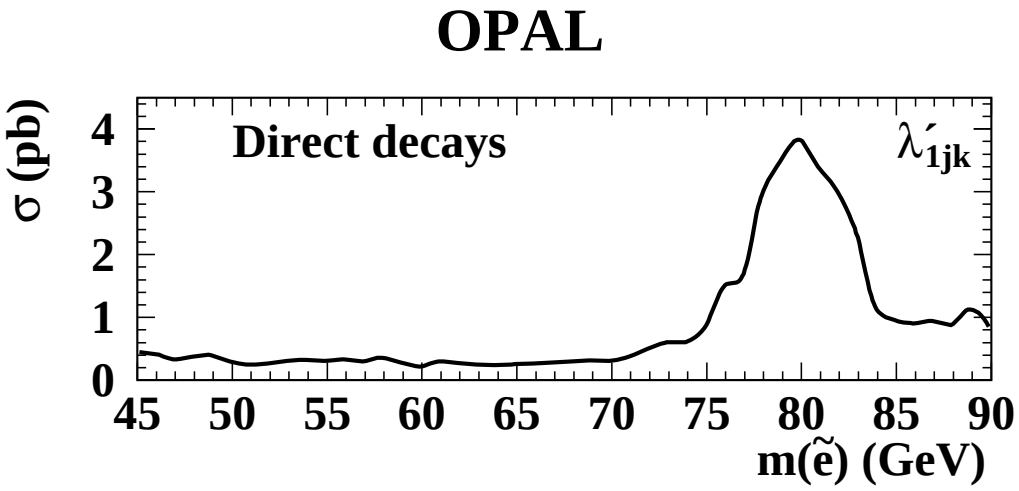

Figure 8: Direct selectron decays via a ^{0} coupling: Upper limits at the 95% C.L. on the pair-production cross-sections of e.

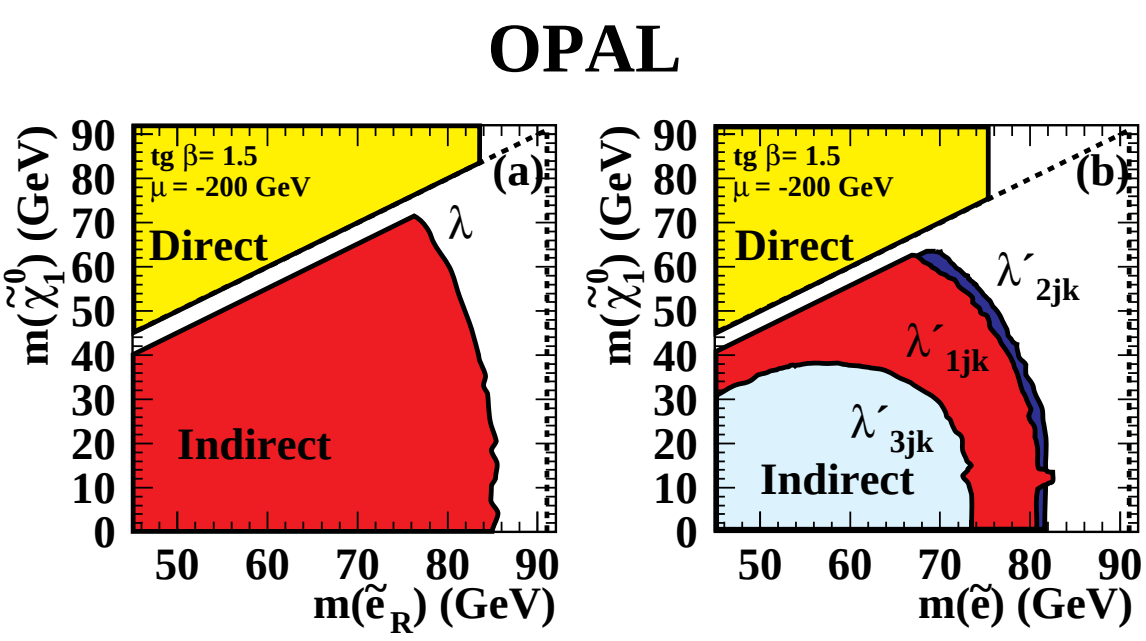

Figure 9: Selectron: MSSM exclusion region for $e^{+}e$ production in the $(m_{e};m_{\tilde{}^{0}_{1}})$ plane at 95% C.L. for (a) a coupling and (b) a ^{0} coupling. For the direct and indirect decays via and the indirect decays via ^{0} the exclusion region for $e_{R}e_{R}$ is shown. For the direct decays via ^{0} the exclusion is shown for the only possible case of $e_{L}e_{L}$. The kinematic limit is shown as the dashed line. The gap between the excluded regions for direct and indirect decays corresponds to $m = m_{\tilde{}} - m_{\tilde{}^{0}_{1}} < 5$ GeV.

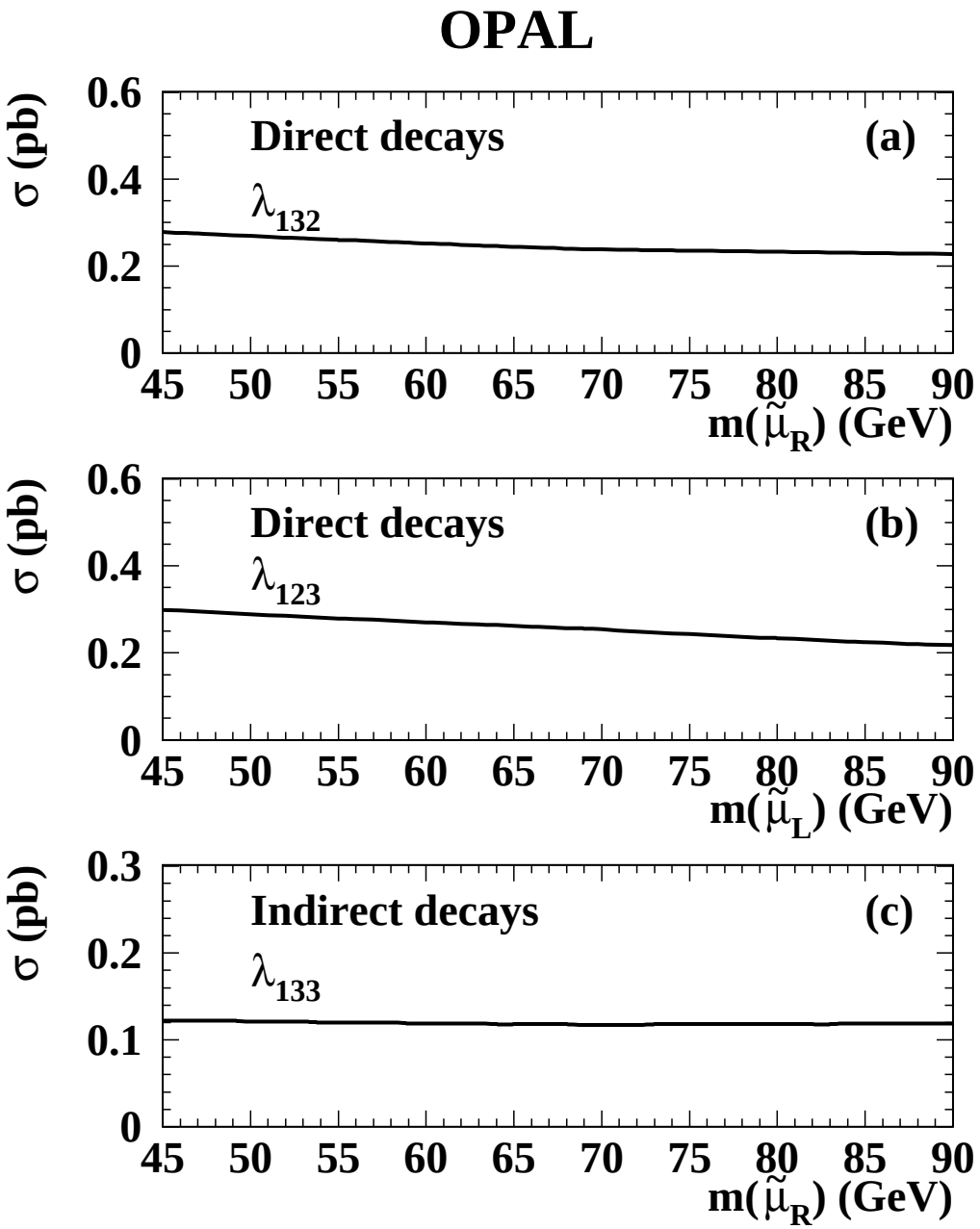

Figure 10: Smuon decays via a coupling: Upper limits at the 95% C.L. on the pair production cross-sections of ~ for (a) the direct decay of a right-handed ~R, (b) the direct decay of a left-handed ~L and (c) the indirect decay of a ~R. Only the worst limit curve is shown and the corresponding to it is indicated.

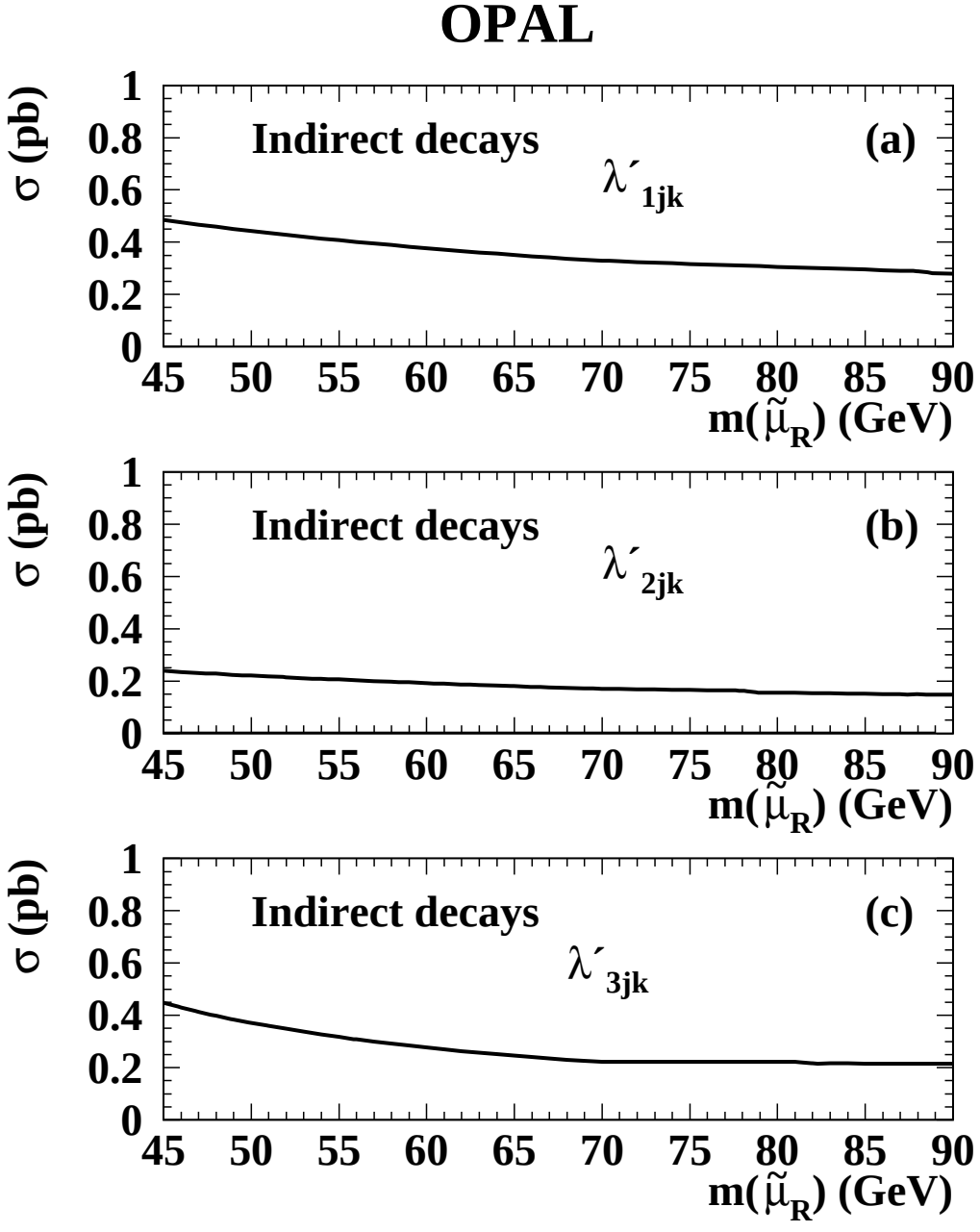

Figure 11: Smuon decays via a ^{0} coupling: Upper limits at the 95% C.L. on the pair-production cross-sections of ~ for (a) the indirect decay of a $\sim_R$ in the electron channel, (b) the indirect decay of a $\sim_R$ in the muon channel and (c) the indirect decay of a $\sim_R$ in the tau channel.

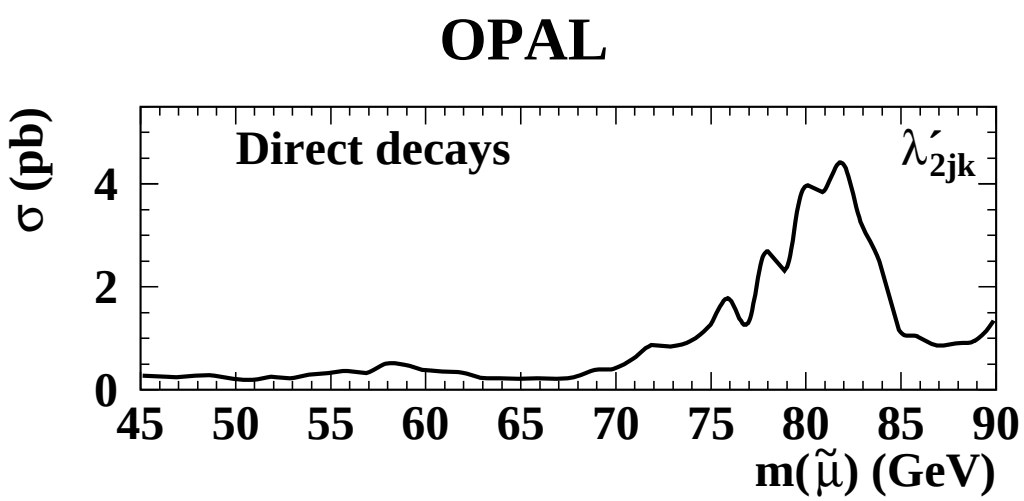

Figure 12: Smuon direct decays via a ^{0} coupling: Upper limits at the 95% C.L. on the pair-production cross-sections of ~.

In the MSSM, for indirect decays via a coupling, a right-handed smuon with a mass smaller than 74 GeV is excluded at the 95% C.L. in the case of a low-mass $\tilde{}^{0}_{1}$, see Figure 13. For direct decays via a coupling, a right-handed smuon with a mass smaller than 66 GeV is excluded at the 95% C.L. For indirect decays via a ^{0} coupling, a right-handed smuon with a mass smaller than 50 GeV is excluded at the 95% C.L. in the case of a low-mass $\tilde{}^{0}_{1}$: for direct decays a left-handed smuon with a mass smaller than 64 GeV is excluded.

10.3 Stau Limits

Figures 14 to 16 show the exclusion plots for pair-produced ~. The weakest upper limit on the cross-section is 0.30 pb for the couplings and 0.45 pb for the ^{0} couplings.

Pair-produced ~ directly decaying via a ^{0} coupling to a four-jet final state yield identical results as shown for the ~ case, see Figure 12.

In the MSSM, for indirect decays via a coupling, a right-handed stau with a mass smaller than 66 GeV is excluded at the 95% C.L. in the case of a low-mass $\tilde{}^{0}_{1}$. For direct decays via a coupling, a right-handed stau with a mass smaller than 66 GeV is excluded at the 95% C.L. For indirect decays via a ^{0} coupling, a right-handed stau with a mass smaller than 66 GeV is excluded at the 95% C.L. in the case of a low-mass $\tilde{}^{0}_{1}$. For direct decays, a left-handed stau with a mass smaller than 63 GeV is excluded.

10.4 Sneutrino Limits

Figures 17 and 18 show the exclusion plots for pair produced ~. The weakest upper limit on the cross-section is 0.52 pb for the couplings and 1.8 pb for the ^{0} couplings.

Figure 19 shows upper limits on the cross-sections of pair-produced ~ decaying directly via a ^{0} coupling to a four-jet final state. The searches for ~ and ~ yield identical limits.

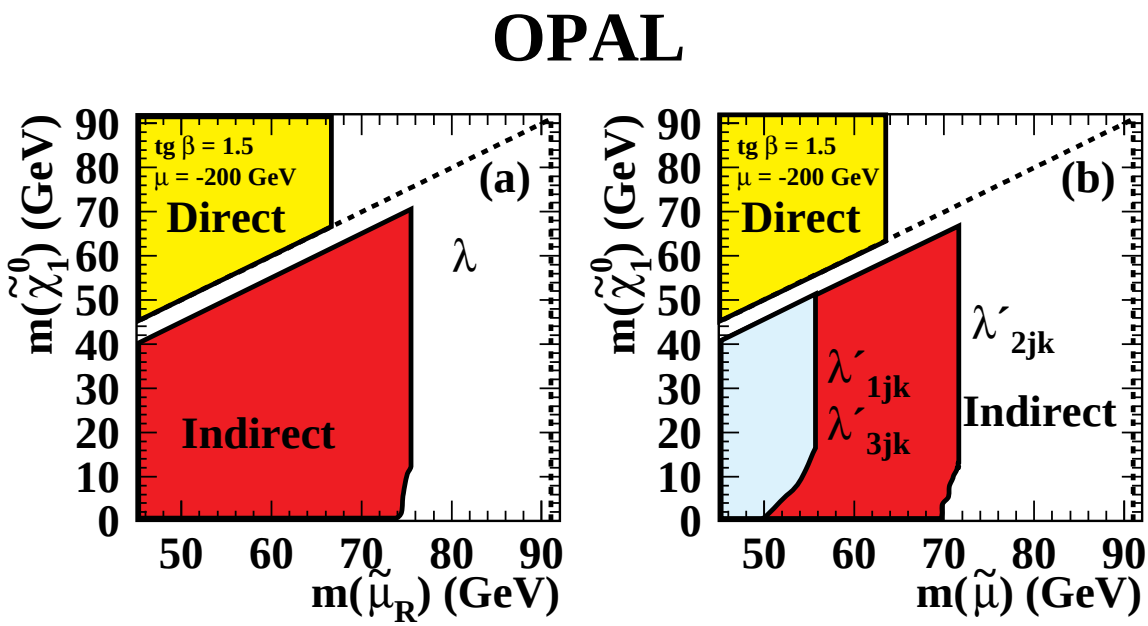

Figure 13: Smuon: MSSM exclusion region for $\tilde{}^{+}\tilde{}$ production in the ($m_{\tilde{}}$;$m_{\tilde{}^0_1}$) plane at 95% C.L. for (a) a coupling and (b) a ^{0} coupling. For the direct decays via ^{0} the exclusion region is shown for the case $\tilde{}_L\tilde{}_L$. In the other cases, the exclusion regions for $\tilde{}_R\tilde{}_R$ are shown. The kinematic limit is shown as the dashed line.

In the MSSM, the $\tilde{}_e$ pair-production cross-section is enhanced by the presence of the t-channel diagram. Figure 20(a) shows the 95% C.L. exclusion limits for $\tilde{}_e$ decaying directly or indirectly via a coupling. For indirect decays via a coupling, an electron sneutrino with a mass smaller than 87 GeV is excluded at the 95% C.L. in the case of a low-mass $\tilde{}^0_1$. For direct decays via a coupling, an electron sneutrino with a mass smaller than 88 GeV is excluded at the 95% C.L. Figure 20 (b) shows the 95% C.L. exclusion limits for electron sneutrinos decaying indirectly via a ^{0} coupling. In this case, an electron sneutrino with a mass smaller than 86 GeV is excluded at the 95% C.L. in the case of a low-mass $\tilde{}^0_1$. For direct decays, a sneutrino with a mass smaller than 80 GeV is excluded. MSSM exclusion plots for $\tilde{}$ and $\tilde{}$ are not shown because of their very small cross-section. For direct $\tilde{}$ decay via a coupling a lower mass limit of 66 GeV is derived. For direct $\tilde{}$ decay via a ^{0} coupling a lower mass limit of 58 GeV is obtained.

10.5 Stop Limits

For the stop search in the electron and muon channel, no events satisfy the final selection cuts. A cross-section limit of 0.15 pb was derived for the pair-production of stops decaying directly via $^0_{13k}$ or $^0_{23k}$, in the mass region 45 GeV < m_t < 90 GeV. The excluded cross-section as a function of the stop mass is shown in Fig. 21 (a). If one assumes a stop production cross-section as predicted by the MSSM, masses lower than 82 GeV can be excluded for any mixing angle $_t$ under the assumptions made above. For the stop search in the tau channel, two events have satisfied the final selection cuts. A cross-section limit of 0.24 pb was derived for the pair-

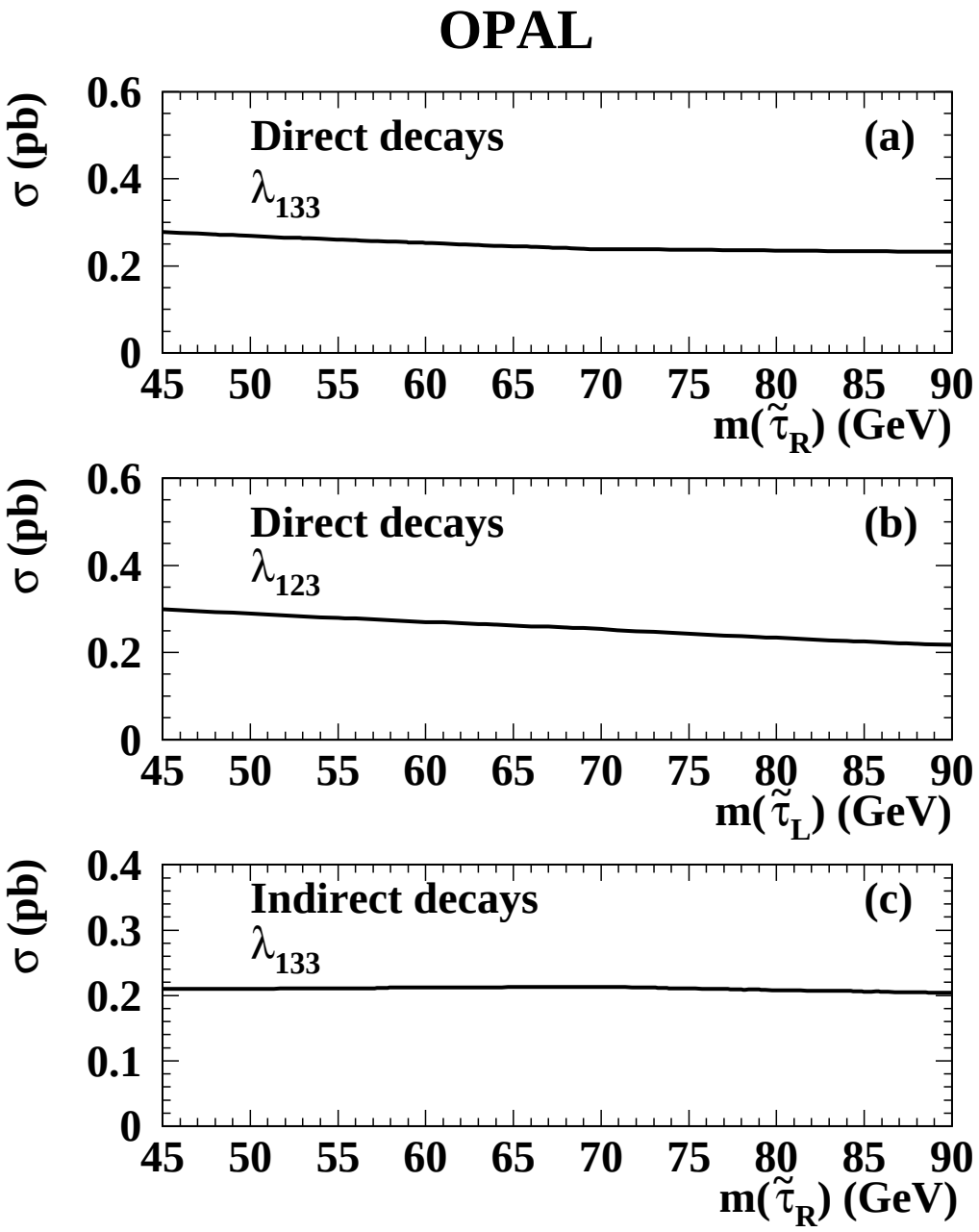

Figure 14: Stau decays via a coupling: upper limits on the pair-production cross-sections for (a) the direct decay of a right-handed $\tilde{\tau}_R$, (b) the direct decay of a left-handed $\tilde{\tau}_L$ and (c) the indirect decay of a $\tilde{\tau}_R$. Only the worst limit curve is shown and the corresponding to it is indicated.

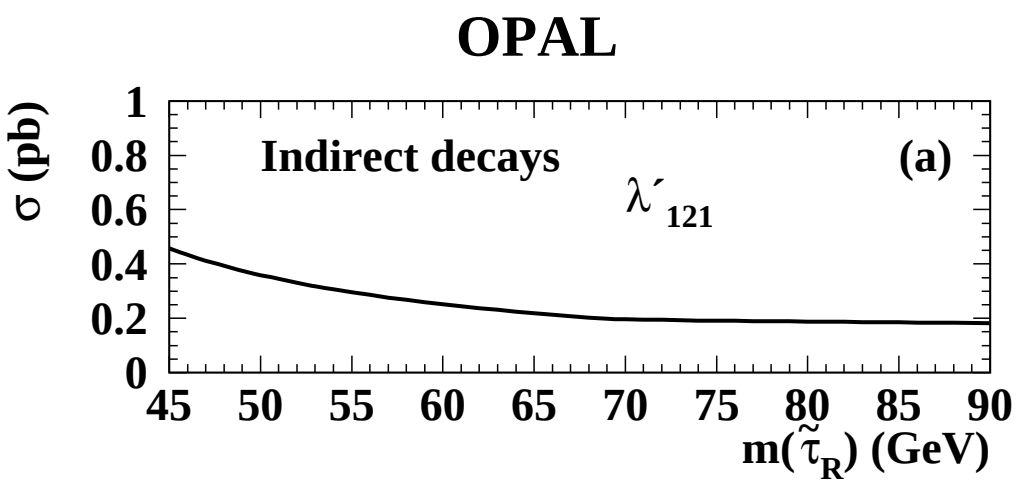

Figure 15: Stau decays via a ^{0} coupling: Upper limits on the pair-production cross-sections for the indirect decay of a $\sim_R$ in the electron channel. The indirect decay of a $\sim_R$ in the muon channel and the indirect decay of a $\sim_R$ in the tau channel yield identical results. Only the worst limit curve is shown and the ^{0} corresponding to it is indicated.

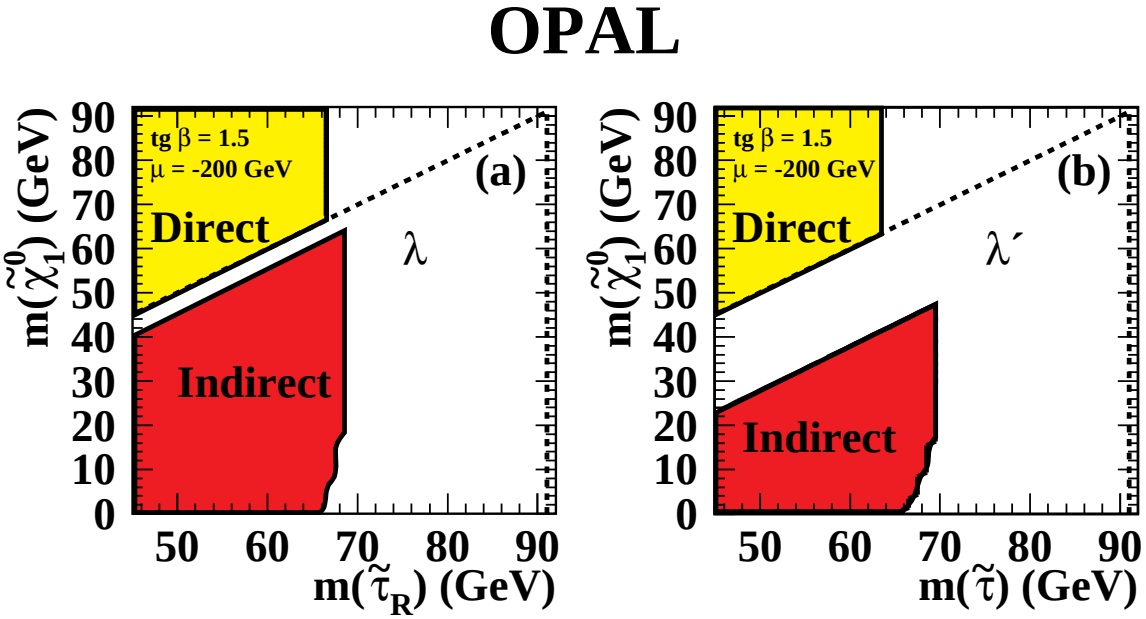

Figure 16: Stau: MSSM exclusion region for $\sim^{+}\sim$ production in the $(m_{\sim};m_{\sim^0_1})$ plane at 95% C.L. for (a) a coupling and (b) a ^{0} coupling. For direct decays via ^{0} the exclusion region for $\sim_L\sim_L$ is shown. In the other cases, exclusion regions for $\sim_R\sim_R$ are shown. The kinematic limit is shown as the dashed line.

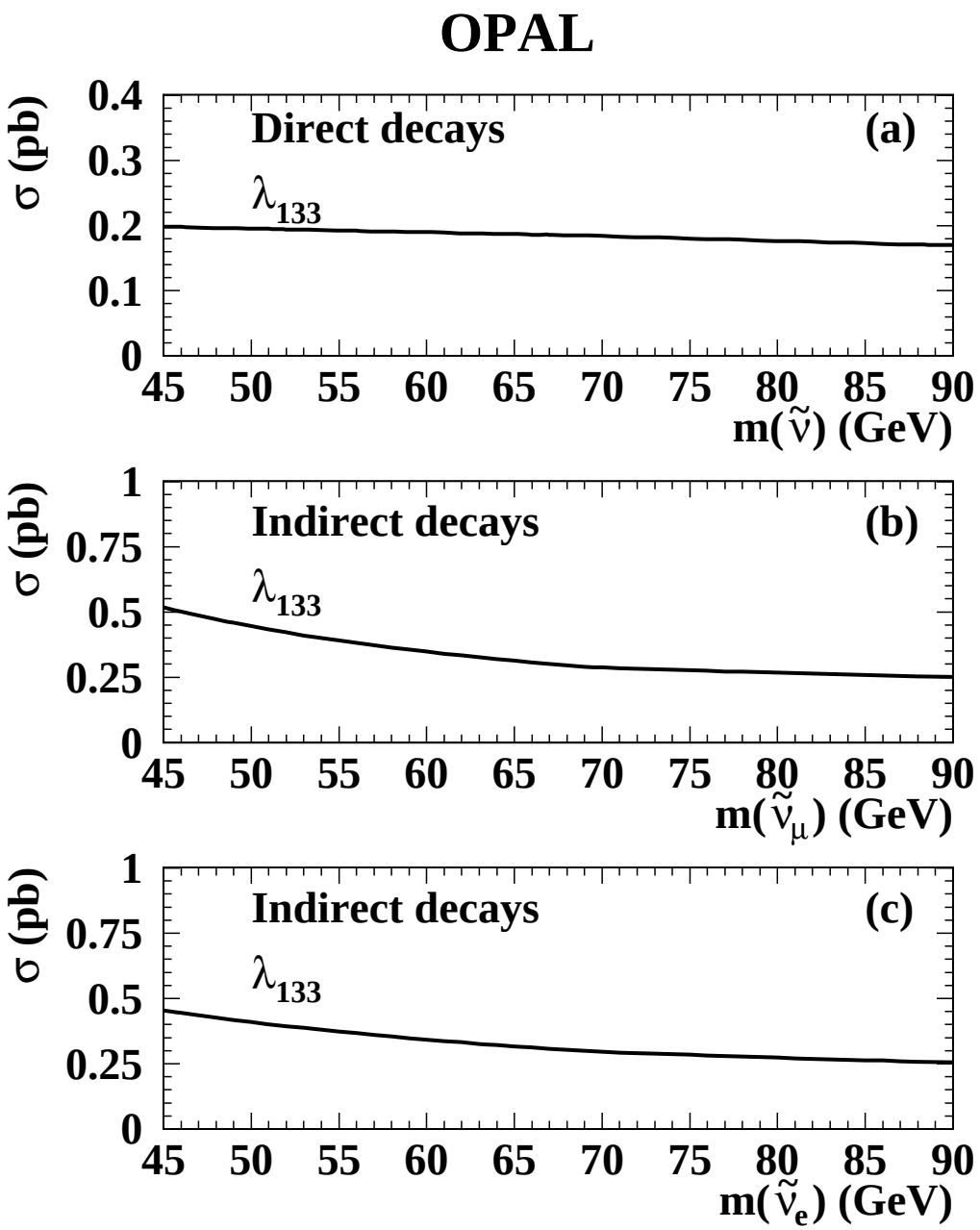

Figure 17: Sneutrino decays via a coupling: Upper limits at the 95% C.L. on the pair-production cross-sections for (a) the direct decay, (b) the indirect decay of ~ (or ~) and (c) the indirect decay of ~$_e$. Only the worst limit curve is shown and the corresponding to it is indicated.

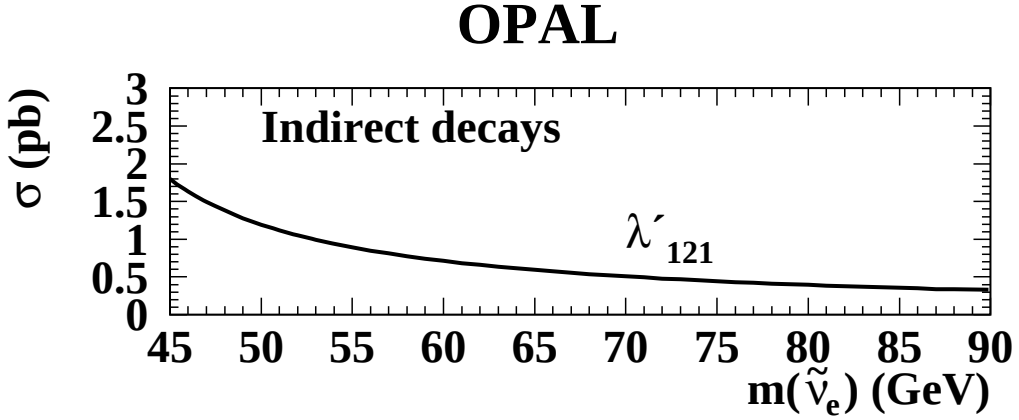

Figure 18: Sneutrino decays via a ^{0} coupling: Upper limits at the 95% C.L. on the pair-production cross-sections. Only the worst limit curve is shown and the ^{0} corresponding to it is indicated.

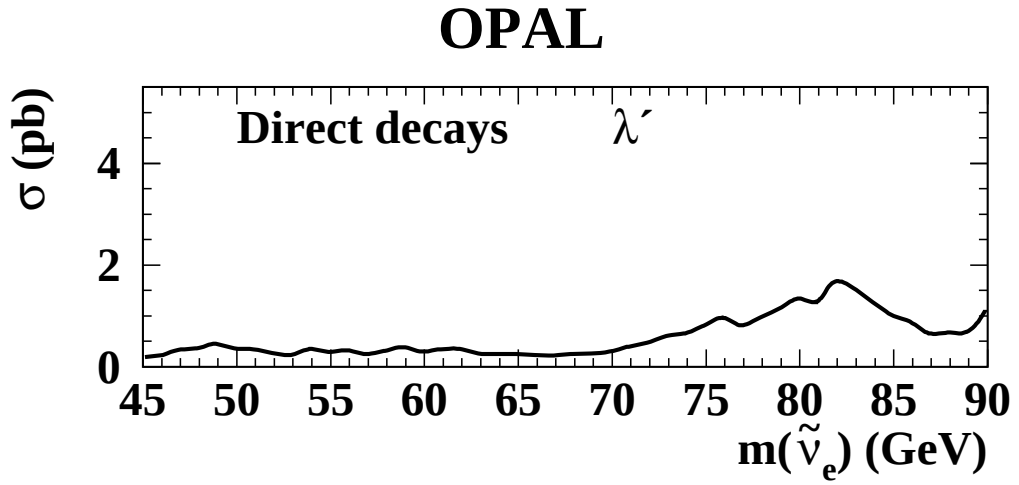

Figure 19: Sneutrino direct decays via a ^{0} coupling: Upper limits at the 95% C.L. on the pair-production cross-sections of $\tilde{\nu}_e$. The search for $\tilde{\ }$ and $\tilde{\ }$ yield identical limits to the ones shown in Figure 12.

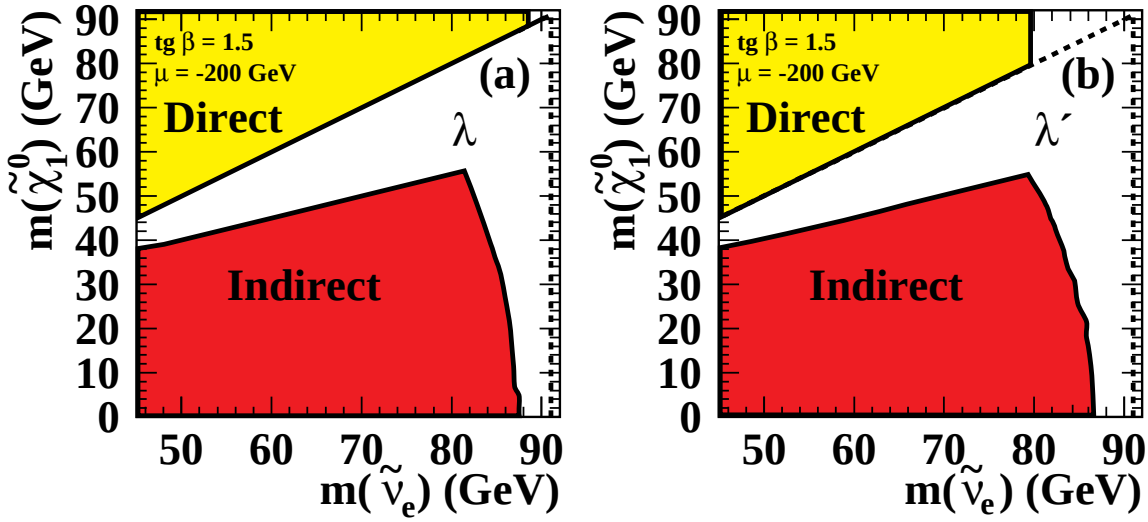

Figure 20: Sneutrino: MSSM exclusion region for $\tilde{}_e \tilde{}_e$ production in the $(m_{\tilde{}_e}; m_{\tilde{}^0_1})$ plane at 95% C.L. for (a) a coupling and (b) a ^{0} coupling. The kinematic limit is shown as the dashed line.

production of the stops decaying directly via $^0_{i3k}$, in the mass region 45 GeV $< m_t <$ 90 GeV. The excluded cross-section as a function of the stop mass is shown in Fig. 21 (b). In the tau channel, masses lower than 73 GeV can be excluded for any mixing angle $_t$. More detailed exclusion limits are given in Table 5.

For the stop decays via ^{00} couplings, 7 events satisfied the selection cuts. A cross-section limit of approximately 0.3 pb was derived for a stop mass up to 75 GeV degrading slightly in the range of the W mass as shown in Fig. 22.

Limits	$_t = 0$ rad	$_t = 0{:}98$ rad
$\tilde{t}_1 \to e + q$	86 GeV	82 GeV
$\tilde{t}_1 \to \quad + q$	86 GeV	82 GeV
$\tilde{t}_1 \to \quad + q$	81 GeV	73 GeV
$\tilde{t}_1 \to qq$	79 GeV	76 GeV

Table 5: Mass limits for stop for the two extreme values of the mixing angle in the electron, muon and tau channels as well as in the 4-jet channel.

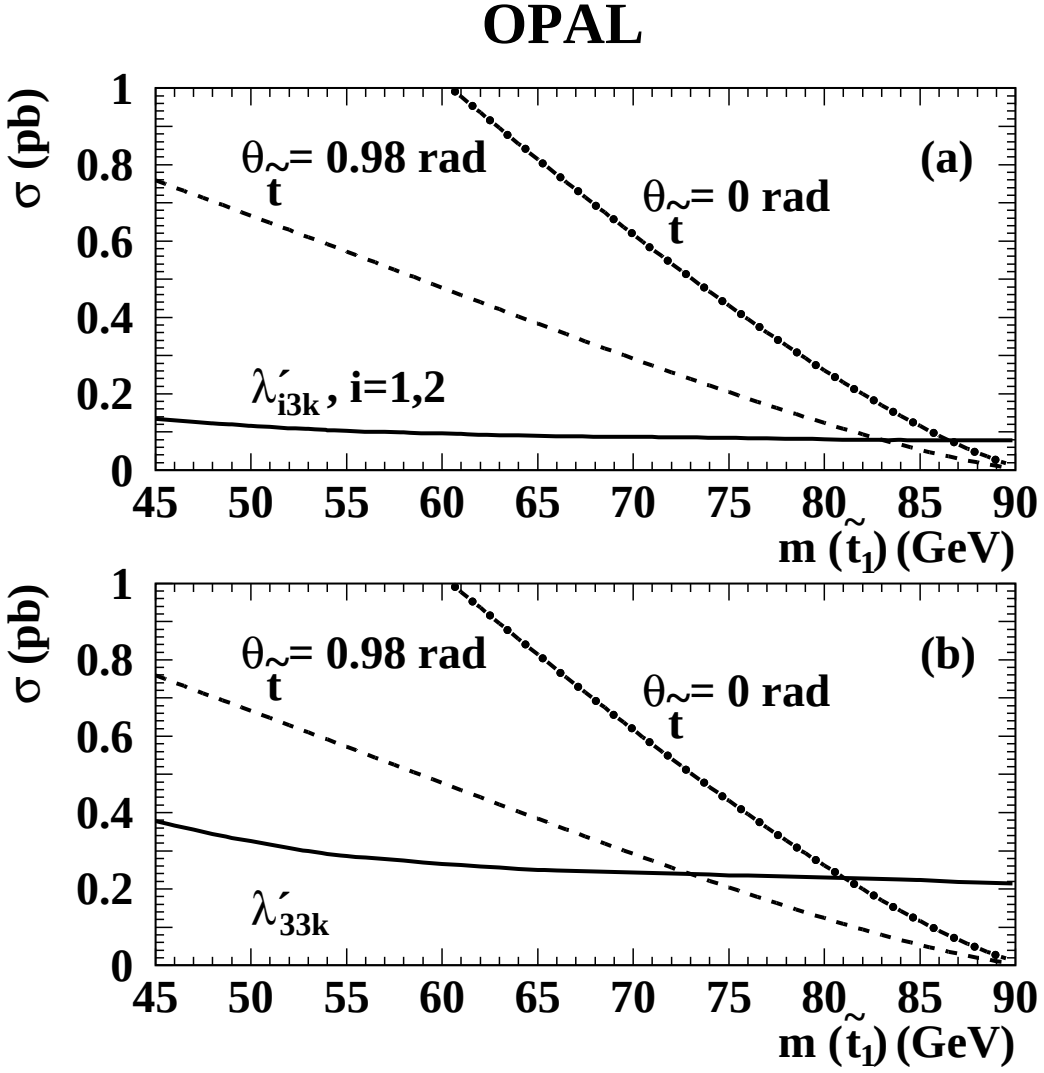

Figure 21: Stop direct decays via a ^{0} coupling: Cross-section limits at the 95% C.L. in the electron and muon channels (a) and in the tau channel (b). Also shown are the maximum (dashed-dotted line) and minimum (dashed line) cross-sections predicted by the MSSM, corresponding to a mixing angle of 0 rad and 0.98 rad (decoupling limit).

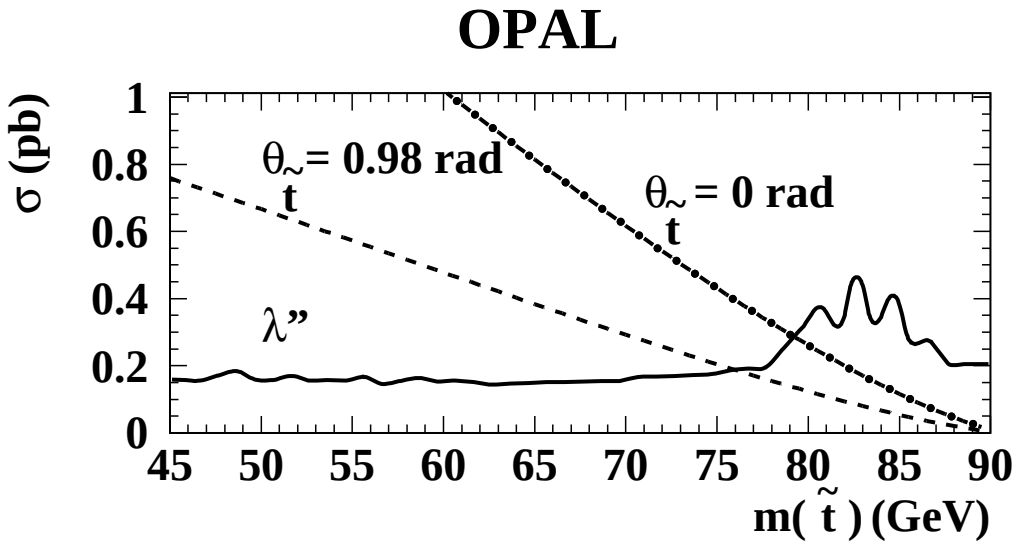

Figure 22: Stop direct decays via a ^{00} coupling: Upper limits at the 95% C.L. on the production cross-section. Also shown are the maximum (dashed-dotted line) and minimum (dashed line) cross-sections predicted by the MSSM, corresponding to a mixing angle of 0 rad and 0.98 rad.

11 Conclusions

We have performed a search for pair produced sfermions with R-parity violating decays using the data collected by the OPAL detector at $\sqrt{s}$ ' 183 GeV corresponding to a luminosity of approximately 56 pb^{1}. Direct and indirect R-parity violating decay modes of $\tilde{\nu}$, $\tilde{}$ via the Yukawa-like and ^{0} couplings as well as direct R-parity violating decay modes of $\tilde{t}$ via ^{0} and ^{00} were considered.

No significant excess of events has been observed in the data. Upper limits on the pair production cross-sections for sfermions have been computed assuming that only R-parity violating decays occur. These cross-section limits, within the MSSM frame used, depend only on the mass of the sfermion and not on other SUSY parameters. Mass limits were derived in the framework of the constrained Minimal Supersymmetric Standard Model whenever the predicted cross-sections were sufficiently large.

Acknowledgements

We particularly wish to thank the SL Division for the efficient operation of the LEP accelerator at all energies and for their continuing close cooperation with our experimental group. We thank our colleagues from CEA, DAPNIA/SPP, CE-Saclay for their efforts over the years on the time-of-flight and trigger systems which we continue to use. In addition to the support staff at our own institutions we are pleased to acknowledge the
Department of Energy, USA,
National Science Foundation, USA,
Particle Physics and Astronomy Research Council, UK,
Natural Sciences and Engineering Research Council, Canada,

Israel Science Foundation, administered by the Israel Academy of Science and Humanities,
Minerva Gesellschaft,
Benoziyo Center for High Energy Physics,
Japanese Ministry of Education, Science and Culture (the Monbusho) and a grant under the
Monbusho International Science Research Program,
Japanese Society for the Promotion of Science (JSPS),
German Israeli Bi-national Science Foundation (GIF),
Bundesministerium fur Bildung, Wissenschaft, Forschung und Technologie, Germany,
National Research Council of Canada,
Research Corporation, USA,
Hungarian Foundation for Scientific Research, OTKA T-016660, T023793 and OTKA F-023259.

References

[1] Y. Golfand and E. Likhtam, JETP Lett. 13 (1971) 323;
D. Volkov and V. Akulov, Phys. Lett. B 46 (1973) 109;
J. Wess and B. Zumino, Nucl. Phys. B 70 (1974) 39.

[2] H.P. Nilles, Phys. Rep. 110 (1984) 1;
H.E. Haber and G.L. Kane, Phys. Rep. 117 (1985) 75.

[3] P. Fayet, in "Unification of the Fundamental Particle Interactions", eds. S. Ferrara, J. Ellis and P. Van Nieuwenhuizen, Plenum Press (1980) 727.

[4] H. Dreiner, "An Introduction to Explicit R-parity Violation", in "Perspectives on Supersymmetry", ed. G.L. Kane (1997) 462, hep-ph/9707435.

[5] OPAL Collab., G. Abbiendi et al., "Searches for R-Parity Violating Decays of Gauginos at 183 GeV at LEP", CERN-EP/98-203, submitted to Eur. Phys. J. C.

[6] ALEPH Collab., R. Barate et al., Eur. Phys. J. C 4 (1998) 433.

[7] ALEPH Collab., R. Barate et al., Eur. Phys. J. C 7 (1999) 383.

[8] G. Bhattacharyya, "R-parity Violating Supersymmetric Yukawa Couplings: a mini-Review," Nucl. Phys. Proc. Suppl. A 52 (1997) 83.

[9] V. Barger, G.F. Giudice and T. Han, Phys. Rev. D 40 (1989) 2987.

[10] K. Agashe and M. Graesser, Phys. Rev. D 54 (1996) 4445.

[11] R.M. Godbole, P. Roy and T. Tata, Nucl. Phys. B 401 (1993) 67.

[12] G. Bhattacharyya, J. Ellis and K. Sridhar, Mod. Phys. Lett. A 10 (1995) 1583.

[13] R.N. Mohapatra, Phys. Rev. D 34 (1986) 3457;
M. Hirsh et al., Phys. Rev. Lett. 75 (1995) 17.

[14] J.L. Goity and M. Sher, Phys. Lett. B 346 (1995) 69.

[15] A.Y. Smirnow and F. Vissani, Phys. Lett. B 380 (1996) 317.

[16] OPAL Collab., K. Ackersta et al., Eur. Phys. J. C 6 (1999) 1.

[17] OPAL Collab., K. Ackersta et al., Phys. Lett. B 433 (1998) 195.

[18] V. Barger, W.-Y. Keung and R.J.N. Phillips, Phys. Lett. B 364 (1995) 27, Erratum-ibid B 377 (1996) 486.

[19] M. Carena et al., Phys. Lett. B 395 (1997) 225.

[20] H. Dreiner, E. Perez and Y. Sirois, in "Future Physics at HERA", eds. G. Ingelman, A. De Roeck, R. Klanner, DESY 96-235, vol.1, p. 295, hep-ph/9703444.

[21] J. Allison et al., Nucl. Instr. Meth. A 317 (1992) 47.

[22] S. Katsanevas and S. Melachroinos, in "Physics at LEP2", eds. G. Altarelli, T. Sjostrand and F. Zwirner, CERN 96-01, vol. 2, p. 328;
S. Katsanevas and P. Morawitz, Comp. Phys. Comm. 112 (1998) 23.

[23] OPAL Collab., K. Ackerstaff et al., Z. Phys. C 75 (1997) 409.

[24] T. Sjostrand and M. Bengtsson, Comp. Phys. Comm. 43 (1987) 367;
"PYTHIA 5.6 and JETSET 7.3, Physics and Manual", CERN-TH. 6488/92;
T. Sjostrand, Comp. Phys. Comm. 82 (1994) 74.

[25] B. Anderson et al., Phys. Rep. 97 (1993) 31.

[26] C. Peterson, D. Schlatter, I. Schmitt and P.M. Zerwas, Phys. Rev. D 27 (1983) 105.

[27] R. Engel and J. Ranft, Phys. Rev. D 54 (1996) 4244;
R. Engel, Z. Phys. C 66 (1995) 203.

[28] G. Marchesini et al., Comp. Phys. Comm. 67 (1992) 465.

[29] R. Bhattacharya, J. Smith and G. Grammer, Phys. Rev. D 15 (1977) 3267;
J. Smith, J.A.M. Vermaseren and G. Grammer, Phys. Rev. D 15 (1977) 3280.

[30] J. Fujimoto et al., Comp. Phys. Comm. 100 (1997) 128.

[31] S. Jadach et al., in "Physics at LEP2", eds. G. Altarelli, T. Sjostrand and F. Zwirner, CERN 96-01, vol.2, p. 229;
S. Jadach, W. Placzek and B.F.L. Ward, Phys. Lett. B 390 (1997) 298.

[32] S. Jadach, B.F.L. Ward and Z. Was, Comp. Phys. Comm. 79 (1994) 503.

[33] OPAL Collab., K. Ahmet et al., Nucl. Instr. Meth. A 305 (1991) 275;
P.P. Allport et al., Nucl. Instr. Meth. A 324 (1993) 34;
P.P. Allport et al., Nucl. Instr. Meth. A 346 (1994) 476.

[34] B.E. Anderson et al., IEEE Transactions on Nuclear Science 41 (1994) 845.

[35] OPAL Collab., R. Akers et al., Z. Phys. C 61 (1994) 19.

[36] OPAL Collab., K. Ackerstaff et al., Phys. Lett. B 396 (1997) 301.

[37] OPAL Collab., M.Z. Akrawy et al., Phys. Lett. B 253 (1991) 511.

[38] OPAL Collab., R. Akers et al., Phys. Lett. B 327 (1994) 411.

[39] OPAL Collab., R. Akers et al., Z. Phys. C 60 (1993) 199.

[40] OPAL Collab., P.D. Acton et al., Z. Phys. C 60 (1993) 19.

[41] OPAL Collab., G. Alexander et al., Z. Phys. C 70 (1996) 357.

[42] OPAL Collab., K. Ackerstaff et al., Phys. Lett. B 389 (1996) 416.

[43] R.D. Cousins and V.L. Highland, Nucl. Instr. Meth. A 320 (1992) 331.

[44] N. Brown and W. J. Stirling, Phys. Lett. B 252 (1990) 657;
S. Bethke, Z. Kunszt, D. Soper and W. J. Stirling, Nucl. Phys. B 370 (1992) 310;
S. Catani et al., Phys. Lett. B 269 (1991) 432;
N. Brown and W. J. Stirling, Z. Phys. C 53 (1992) 629.

[45] OPAL Collab., K. Ackersta et al., Eur. Phys. J. C 6 (1999) 225.

[46] M. G. Bowler, Z. Phys. C 11 (1981) 169.

[47] OPAL Collab., K. Ackersta et al., Eur. Phys. J. C 1 (1998) 425.

[48] OPAL Collab., K. Ackersta et al., Eur. Phys. J. C 5 (1998) 19.

[49] OPAL Collaboration, K. Ackersta et al., Phys. Lett. B 391 (1997) 221.

[50] OPAL Collab., G. Abbiendi et al., Eur. Phys. J. C 7 (1999) 407.

[51] OPAL Collab., K. Ackersta et al., Eur. Phys. J. C 2 (1998) 441.

[52] R. K. Ellis, D. A. Ross and A. E. Terrano, Nucl. Phys. B 178 (1981) 421.

[53] OPAL Collab., G. Alexander et al., Phys. Lett. B 376 (1996) 232.

[54] E. Accomando et al., , in "Physics at LEP2", eds. G. Altarelli, T. Sjostrand and F. Zwirner, CERN 96-01, vol. 2, 299.

[55] OPAL Collab., K. Ackersta et al., Phys. Lett. B 426 (1998) 180.

[56] A. G. Frodesen, O. Skeggestad, and H. Tofte, "Probability and Statistics in Particle Physics", Universitetsforlaget, 1979, ISBN 82-00-01-01906-3;
S. L. Meyer, "Data Analysis for Scientists and Engineers", John Wiley and Sons, 1975, ISBN 0-471-59995-6.